CHEMISTRY
A EUROPEAN JOURNAL

FULL PAPER

DOI: 10.1002/chem.201200868

Phenalenyl-Based Organozinc Catalysts for Intramolecular Hydroamination Reactions: A Combined Catalytic, Kinetic, and Mechanistic Investigation of the Catalytic Cycle

Arup Mukherjee,[a] Tamal K. Sen,[a] Pradip Kr. Ghorai,[a] Prinson P. Samuel,[b] Carola Schulzke,[c] and Swadhin K. Mandal*[a]

Dedicated to Prof. B. M. Deb on the occasion of his 70th birthday

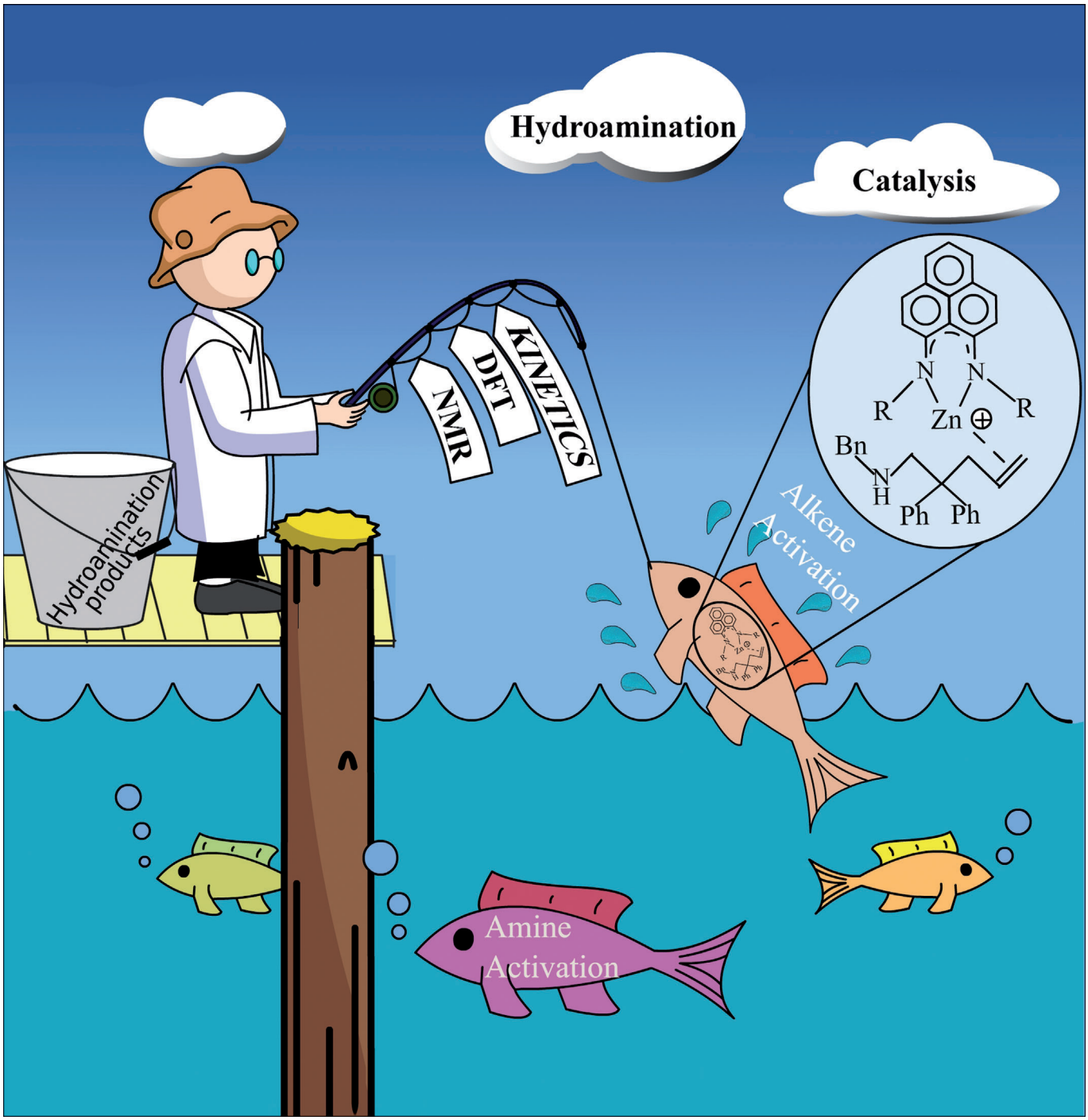

Abstract: Herein, we report the synthesis and characterization of two organozinc complexes that contain symmetrical phenalenyl (PLY)-based N,N-ligands. The reactions of phenalenyl-based ligands with $ZnMe_2$ led to the formation of organozinc complexes [*N*(Me),*N*(Me)-PLY]ZnMe (**1**) and [*N*-(*i*Pr),*N*(*i*Pr)-PLY]ZnMe (**2**) under the evolution of methane. Both complexes (**1** and **2**) were characterized by NMR spectroscopy and elemental analysis. The solid-state structures of complexes **1** and **2** were determined by single-crystal X-ray crystallography. Complexes **1** and **2** were used as catalysts for the intramolecular hydroamination of unactivated primary and secondary aminoalkenes. A combined approach of NMR spectroscopy and DFT calculations was utilized to obtain better insight into the mechanistic features of the zinc-catalyzed hydroamination reactions. The progress of the catalysis for primary and secondary aminoalkene substrates with catalyst **2** was investigated by detailed kinetic studies, including kinetic isotope effect measurements. These results suggested pseudo-first-order kinetics for both primary and secondary aminoalkene activation processes. Eyring and Arrhenius analyses for the cyclization of a model secondary aminoalkene substrate afforded $\Delta H^{\neq} = 11.3\ \text{kcal mol}^{-1}$, $\Delta S^{\neq} = -35.75\ \text{cal K}^{-1}\text{mol}^{-1}$, and $E_a = 11.68\ \text{kcal mol}^{-1}$. Complex **2** exhibited much-higher catalytic activity than complex **1** under identical reaction conditions. The in situ NMR experiments supported the formation of a catalytically active zinc cation and the DFT calculations showed that more active catalyst **2** generated a more stable cation. The stability of the catalytically active zinc cation was further supported by an in situ recycling procedure, thereby confirming the retention of catalytic activity of compound **2** for successive catalytic cycles. The DFT calculations showed that the preferred pathway for the zinc-catalyzed hydroamination reactions is alkene activation rather than the alternative amine-activation pathway. A detailed investigation with DFT methods emphasized that the remarkably higher catalytic efficiency of catalyst **2** originated from its superior stability and the facile formation of its cation compared to that derived from catalyst **1**.

Keywords: density functional calculations · homogeneous catalysis · hydroamination · phenalenyl ligands · zinc

Introduction

The hydroamination reaction, which involves the addition of an amine across a carbon–carbon multiple bond, leads to the formation of nitrogen-containing heterocyclic molecules.[1] The synthesis of these nitrogen-containing molecules is of particular interest in academia, as well as in industry, because these nitrogen-containing molecules are important as natural products, pharmacological agents, fine chemicals, and dyes. At present, most of these molecules are synthesized by using multistep procedures. However, hydroamination offers an alternative strategy to synthesize these nitrogen-containing molecules in a more environmentally friendly and atom-economical way. Over the last decade, there has been an enormous effort to develop an efficient catalyst for this demanding transformation. Several catalyst systems, which are composed of main-group elements,[2] rare-earth metals,[3] and transition metals,[4] have been used successfully to carry out such transformations.[1] In this context, there has been a growing trend to use low-cost, non-toxic metals, such as zinc, in the hydroamination reaction. Zinc is an essential, non-toxic, and environmentally friendly metal, as shown by the presence of about 2 g of zinc ions in the body of an adult human.[5] In 2005, Roesky, Blechert, and coworkers first reported the use of an organozinc complex, [*N*-isopropyl-2-(isopropylamino)troponiminato]methylzinc [{(iPr)$_2$ATI}-ZnMe] (ATI = aminotroponiminato), as a catalyst for the hydroamination of aminoalkenes and aminoalkynes.[6a] They found that the use of an activator, $[PhNMe_2H][B(C_6F_5)_4]$, dramatically enhances the catalytic activity of the organozinc catalyst. The activator abstracts the alkyl group that is attached to zinc, thereby generating the active cationic zinc intermediate.[6b] Following this study, several efforts have been made in recent years that use zinc-based catalysts for intramolecular hydroamination reactions.[6] However, the exact mechanistic pathway for zinc-catalyzed hydroamination reactions has not yet been elucidated in detail. In principle, there are two possible mechanisms for the zinc-catalyzed hydroamination reaction: 1) activation of the C–C multiple bond followed by nucleophilic attack by the amine moiety or 2) activation of the amine, which results in a metal–amide complex, followed by an olefin-insertion reaction (Scheme 1).[1f,6b] Several studies have reported that hydroamination reactions with lantha-

[a] A. Mukherjee, T. K. Sen, Dr. P. K. Ghorai, Dr. S. K. Mandal
Department of Chemical Sciences
Indian Institute of Science Education and
Research-Kolkata
Mohanpur-741252 (India)
Fax: (+91) 33-48092033
E-mail: swadhin.mandal@iiserkol.ac.in
[b] Dr. P. P. Samuel
Institut für Anorganische Chemie
Georg-August Universität Göttingen
Tammannstrasse 4, 37077 (Germany)
[c] Dr. C. Schulzke
School of Chemistry, Trinity College Dublin
Dublin 2 (Ireland)

Supporting information for this article is available on the WWW under http://dx.doi.org/10.1002/chem.201200868.

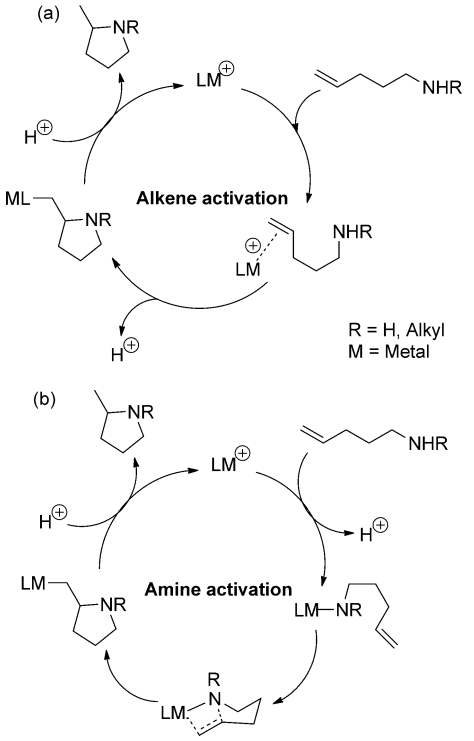

Scheme 1. Plausible mechanistic pathways for the zinc-catalyzed intramolecular hydroamination reactions.

nides, early transition metals, and Group 2-metal-based catalysts proceed through the activation of the N–H bond.[1g,2d,4a,d] On the other hand, late-transition-metal-based catalysts promote C–C multiple bond activation with concomitant attack by the nitrogen nucleophile.[4k,o] However, it has not yet been established exactly which of the two mechanistic pathways is operative in the case of the zinc-catalyzed hydroamination reaction.[6b,o]

As a part of our ongoing interest in the development of hydroamination catalysts, we recently reported that a heterobimetallic complex, based on Group 2 and Group 4 metals, can successfully cyclize both unactivated primary and secondary aminoalkenes in a dual fashion.[7] Herein, we report the use of phenalenyl-based ligands for developing organozinc hydroamination catalysts. Phenalenyl is a well-known odd-alternant hydrocarbon with high symmetry (D_{3h}) that has been used as a building block for preparing intriguing materials as new conjugated electronic systems, such as multifunctional electronic and magnetic materials, that exhibit simultaneous bistability in multiple physical channels and the highest room-temperature conductivity of any neutral organic solids.[8] Recent articles by Morita, Takui, and coworkers, and by Hicks, document the state-of-the-art status of phenalenyl-based materials chemistry.[9] Recently, we initiated a program with phenalenyl-based ligands for designing molecular catalysts[10] because phenalenyl systems may have similarities to the well-studied aminotroponimate ligand system in terms of their metal-binding ability.[11] We utilized density functional theory (DFT) calculations, as well as detailed kinetic studies by NMR spectroscopy, to understand the mechanistic pathway for the zinc-catalyzed hydroamination reaction. Herein, we report the synthesis and characterization of two organozinc complexes, [*N*(Me),*N*(Me)-PLY]ZnMe (**1**) and [*N*(*i*Pr),*N*(*i*Pr)-PLY]ZnMe (**2**), that contain symmetrical phenalenyl (PLY)-based N,N-ligands. The catalytic activity of complex **2** was remarkably higher than that of complex **1**. DFT calculations disclosed that the formation and stability of cations from these organozinc complexes play a key role in their relative catalytic activity. To better understand the catalytic cycle, more-detailed DFT calculations were carried out on the key intermediates in the reaction, as well as on various transition states (TSs). These calculations reveal that such transformations proceed through an olefin-activation mechanism. Kinetic studies, including kinetic isotope effects, were carried out on the cyclization of primary and secondary aminoalkenes by using catalyst **2**, which showed pseudo-first-order kinetics in the cyclization process.

Results and Discussion

Synthesis of organozinc complexes: The syntheses of [*N*(Me),*N*(Me)-PLY]ZnMe (**1**) and [*N*(*i*Pr),*N*(*i*Pr)-PLY]ZnMe (**2**) were accomplished by reacting 9-*N*-methylamino-1-*N*′-methyliminophenalene [H*N*(Me),*N*(Me)-PLY] and 9-*N*-isopropylamino-1-*N*′-isoproyliminophenalene [H*N*-(*i*Pr),*N*(*i*Pr)-PLY] with $ZnMe_2$ at 25 °C and 110 °C, respectively (Scheme 2). A solution of [H*N*(Me),*N*(Me)-PLY] or [H*N*(*i*Pr),*N*(*i*Pr)-PLY] in toluene was added drop-by-drop to a solution of $ZnMe_2$ in toluene in a 1:1.2 stoichiometric ratio at −78 °C, and the mixture was stirred at 25 °C for 3 h (for **1**) or heated at 110 °C for 24 h (for **2**) to yield complex **1** or **2**. The ^{1}H NMR spectra of both mixtures reveal clean and almost-quantitative conversion of the reactants into the products, which can be concluded from the absence of any characteristic N–H resonance at $\delta = 13.1$ or 13.7 ppm in C_6D_6, respectively. Complexes **1** and **2** were characterized by ^{1}H and ^{13}C NMR spectroscopy and elemental analysis. The solid-state structures of complexes **1** and **2** were determined by single-crystal X-ray crystallography. The ^{1}H NMR spectra of complexes **1** and **2** in C_6D_6 exhibited singlets at

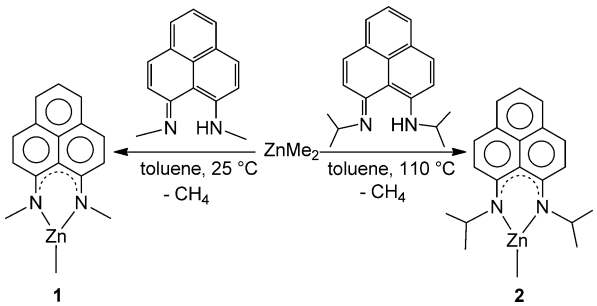

Scheme 2. Synthesis of organozinc complexes **1** and **2** with phenalenyl ligands.

$\delta = -0.20$ and 0.04 ppm, respectively, which are due to the proton resonances that arise from the methyl group that is bound to the zinc center. The Zn−Me resonance is shifted upfield in both complexes **1** and **2** when compared to that in $ZnMe_2$ ($\delta = 0.51$ ppm).[6k] The ^{13}C NMR spectra of complexes **1** and **2** reveal resonances at $\delta = -4.3$ and -5.9 ppm, respectively, which are due to the methyl carbon atom that is bound to the zinc center; this resonance is also shifted further upfield than that in $ZnMe_2$ ($\delta = -4.2$ ppm).[6k]

X-ray crystal structures of complexes 1 and 2: Crystals of complexes **1** and **2** were obtained from solutions in toluene at 0°C and 25°C, respectively. The molecular structures were determined by single-crystal X-ray crystallography (Figure 1). Complexes **1** and **2** crystallized in the triclinic space group $P\bar{1}$ with one and two molecules in the asymmetric unit, respectively. The X-ray structures of complexes **1** and **2** reveal a trigonal-planar geometry around the zinc center, with two nitrogen atoms of the phenalenyl ligand and one carbon atom of the methyl group coordinated to zinc. The Zn−N distances in complexes **1** (Zn1−N1 1.929(2) Å, Zn1−N2 1.9353(19) Å) and **2** (Zn1−N1 1.954(2) Å, Zn1−N2 1.954(2) Å) are comparable to the distances in [*N*-isopropyl-2-(isopropylamino)troponiminato]-methylzinc (1.96 Å).[6a] The N-Zn-C bond angles in complexes **1** (average 132.2°) and **2** (average 133.3°) are smaller than those in [*N*-isopropyl-2-(isopropylamino)troponiminato]methylzinc (N-Zn-C average 139.05°),[6a] thereby making the N1-Zn1-N2 bond angles (95.48(8)° in **1** and 93.34(9)° in **2**) wider than that in [*N*-isopropyl-2-(isopropylamino)troponiminato]methylzinc (81.94°).[6a] The Zn−C distances in complexes **1** (1.954(3) Å) and **2** (1.955(3) Å) are within the expected range that was observed in previously characterized methylzinc complexes.[6a,o] The C−N distances in complexes **1** (average 1.333 Å) and **2** (average 1.334 Å) are in between the C=N double-bond (1.270 Å)[12] and C−N single-bond lengths (1.485 Å).[12] In the solid state, the molecules of complexes **1** and **2** are packed into layers, owing to their planar geometry, with the phenalenyl moiety maximizing the intermolecular interactions (see the Supporting Information).

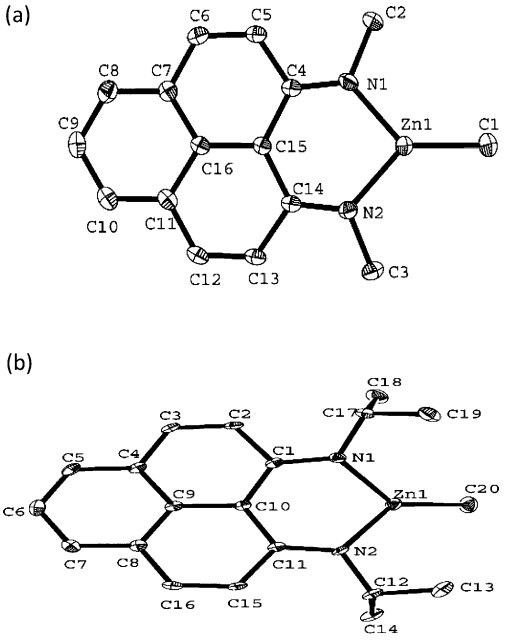

Figure 1. Molecular structures of organozinc complexes a) **1** and b) **2**; thermal ellipsoids are set at 50% probability level and hydrogen atoms are omitted for the sake of clarity. Selected distances [Å] and angles [°] in complex **1**: Zn1−N1 1.929(2), Zn1−N2 1.9353(19), Zn1−C1 1.954(3), N1−C2 1.472(3), N2−C3 1.468(3), N1−C4 1.335(3), N2−C14 1.331(3); N1-Zn1-C1 131.54(10), N2-Zn1-C1 132.90(10), N1-Zn1-N2 95.48(8), C2-N1-Zn1 114.90(15), C3-N2-Zn1 114.84(15), C4-N1-Zn1 126.06(15), C14-N2-Zn1 126.26(15). Selected distances [Å] and angles [°] in complex **2**: Zn1−N1 1.954(2), Zn1−N2 1.954(2), Zn1−C20 1.955(3), N1−C1 1.333(3), N1−C17 1.478(4), N2−C11 1.335(3), N2−C12 1.481(3); N1-Zn1-C20 133.70(12), N2-Zn1-C20 132.89(12), N1-Zn1-N2 93.34(9), C1-N1-Zn1 120.42(18), C11-N2-Zn1 122.67(19), C17-N1-Zn1 116.93(17), C12-N2-Zn1 115.24(17).

Catalytic intramolecular hydroamination reactions: The increasing demand for efficient catalysts for the hydroamination reaction prompted us to test the catalytic activity of complexes **1** and **2** for intramolecular hydroamination reactions. Previous studies have demonstrated that organozinc-based complexes can catalyze the intramolecular hydroamination of aminoalkenes.[6a–c,l,o] Recent developments have established that organozinc complexes, such as [*N*-isopropyl-2-(isopropylamino)troponiminato]methylzinc [{(*i*Pr)$_2$ATI}-ZnMe] (ATI = aminotroponiminato) and [2-(isopropylamino)troponate]methylzinc [(*i*PrAT)Zn-Me]$_2$ (AT = aminotroponate), can catalyze the hydroamination of primary aminoalkenes.[6a,n] The successful synthesis of complexes **1** and **2**, which contain a methylzinc moiety, gave us the opportunity to test their efficacy for the intramolecular hydroamination of aminoalkenes.

Intramolecular hydroamination of primary aminoalkenes: We began our study with unactivated primary aminoalkenes. Initially, we performed the intramolecular hydroamination reaction of (1-allylcyclohexyl)methylamine (**3**) with complexes **1** and **2** in C_6D_6 whilst maintaining the bath temperature at 120°C without adding any activator. After heating for 24 h, we found <5% of the hydroamination product with complex **2** and no detectable resonances of the hydroamination product in the ^1H NMR spectrum with complex **1**. To increase the catalytic activity of complexes **1** and **2** towards primary aminoalkenes, the reaction was carried out with an equimolar amount (with respect to the catalyst) of the activator [PhNMe$_2$H][B(C$_6$F$_5$)$_4$]; we found that, after 8.5 h at 120°C in C_6D_6, catalyst **2** afforded 91% conversion. This increase in activity may be attributed to the in situ generation of the coordinatively unsaturated cationic zinc species, in which the activator acts as a methyl-abstracting agent. Earlier studies on the zinc-catalyzed hydroamination reaction have established the role of an externally added activator, indicating the formation of catalytically active cationic species.[6a–c,o] The reactions of catalysts **1** and **2** with dry and degassed primary aminoalkenes proceeded regio-

specifically. All of the substrates were converted into their corresponding cyclic products by using 5 mol% loading of the catalyst and activator at 120°C in C_6D_6.

The catalytic activities of complexes **1** and **2** with different aminoalkenes are summarized in Table 1. Examination of the data emphasizes that catalyst **2** has a much higher activity than catalyst **1** under identical reaction conditions. In addition, substrates that contain bulky substituents at the β position with respect to the amine moiety (Thorpe–Ingold effect) are transformed into their corresponding heterocyclic products more swiftly (Table 1, entries 2 and 4). 2,2-Diphenylpent-4-en-1-amine (Table 1, entry 2) was the most reactive substrate, thereby forming its corresponding pyrrolidine within 7.5 h; the yield of isolated product after column chromatography was 90% with catalyst **2**, which was in good agreement with that observed by ^{1}H NMR spectroscopy. In the case of (1-allylcyclohexyl)methylamine (**3**; Table 1, entry 4), 8.5 h were necessary to achieve 91% conversion. Substitution with a methyl group at the internal position of the olefin moiety had a significant negative impact on the reaction rate (Table 1, entries 7–10) and difficulties in cyclization, for example, resulting in the conversion of 4-methyl-2,2-diphenylpent-4-en-1-amine into 2,2-dimethyl-4,4-diphenylpyrrolidine taking 96 h at 120°C (Table 1, entry 8). In situ NMR studies of the cyclization of compound **3** with catalyst **2** in C_6D_6 at 120°C revealed a clean conversion of the substrate to afford heterocyclic hydroamination product **4**. Figure 2 shows that the resonances of the olefinic protons of the aminoalkene moiety disappear with time, whilst the protons that correspond to the hydroamination product grow.

Table 1. Intramolecular hydroamination of unactivated primary aminoalkenes.[a]

	Substrate	Product	Cat.	*t* [h]	Conv. [%][b]
1	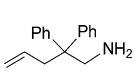	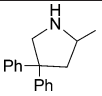	**1**	7.5	12
2			**2**		98(90)[c]
3	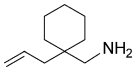	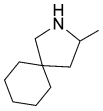	**1**	8.5	15
4			**2**		91
5	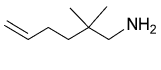		**1**	24	2
6			**2**		97
7	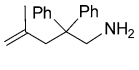	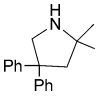	**1**	96	12
8			**2**		98
9	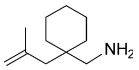	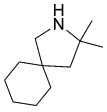	**1**	110	14
10			**2**		97

[a] Reaction conditions: amine (20 μL), catalyst (5 mol%), and activator $[PhNMe_2H][B(C_6F_5)_4]$ (5 mol%) in C_6D_6 (0.6 mL) at 120°C. [b] Determined by ^{1}H NMR spectroscopy against an internal standard. [c] Yield of isolated product after purification. Cat. = catalyst; Conv. = conversion.

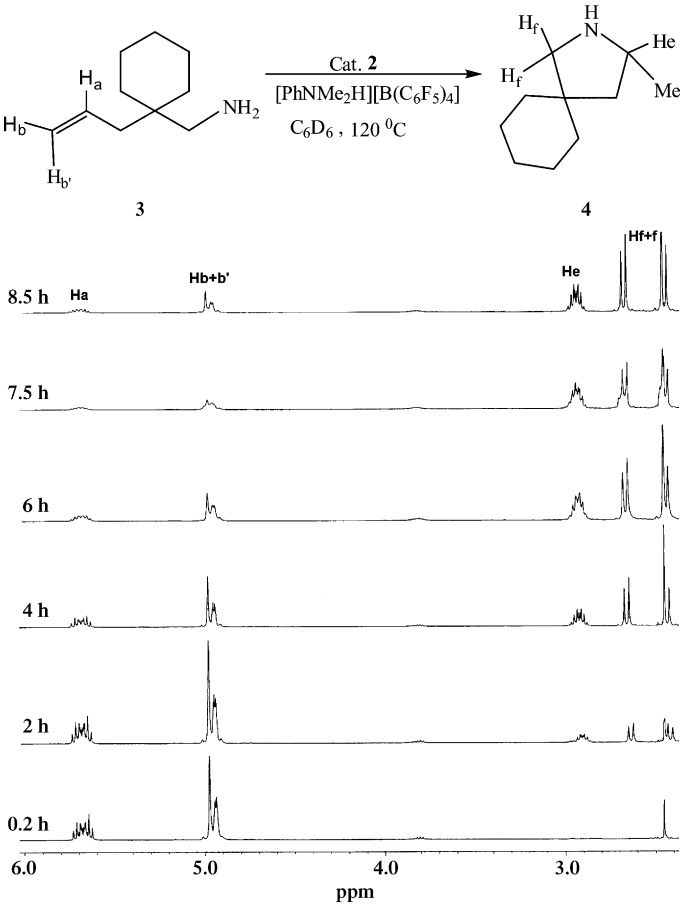

Figure 2. Stacked ^{1}H NMR spectra (C_6D_6) for the cyclization of (1-allylcyclohexyl)methylamine (**3**) with catalyst **2** after certain time intervals.

The higher catalytic activity of complex **2** compared to complex **1** may be attributed to the electronic stability of the in-situ-generated zinc cation (see later). Complex **2** showed comparable or higher activity than that of a previously reported organozinc complex in the presence of an activator.[6a,n]

Intramolecular hydroamination of secondary aminoalkenes: Based on the promising reactivity displayed by complex **2** towards primary aminoalkenes, we postulated that it would also be effective for the intramolecular hydroamination of unactivated secondary aminoalkenes. To test the catalytic activities of compounds **1** and **2** towards secondary aminoalkenes, we performed the catalytic reactions with a number of secondary aminoalkenes in C_6D_6 at 80°C with 5 mol% loading of the catalyst and activator (Table 2). 4-(Bromobenzyl)(2,2-diphenyl-4-pentenyl)amine (Table 2, entries 1 and 2) cyclized efficiently with 99% conversion within 2.5 h by using catalyst **2** and an equimolar amount of the activator, whilst the conversion with catalyst **1** under identical conditions was only 5%. The yield of isolated product after column chromatography (Table 2, entry 2) was 92% with catalyst **2**, which is in good agreement with the conversion that was observed by ^{1}H NMR spectroscopy of the reaction

Table 2. Intramolecular hydroamination of unactivated secondary aminoalkenes.[a]

	Substrate	Product	Cat.	*t* [h]	Conv. [%][b]
1	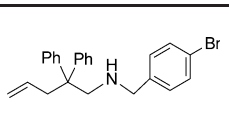	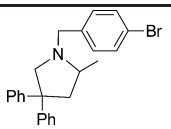	**1**	2.5	5
2			**2**		99(92)[c]
3	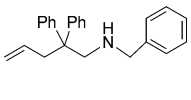	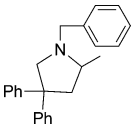	**1**	4.0	8
4[d]			**2**		96
5	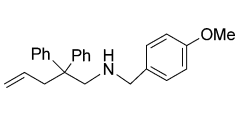	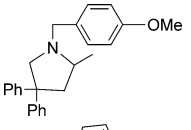	**1**	2.5	6
6			**2**		98
7	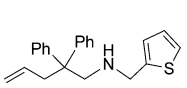	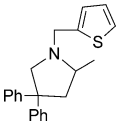	**1**	0.5	3
8			**2**		99
9	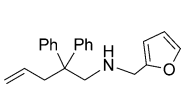	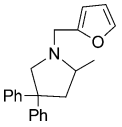	**1**	2.5	5
10			**2**		99
11	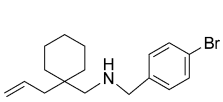	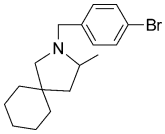	**1**	3.5	12
12			**2**		97
13	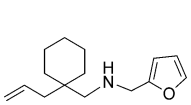	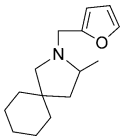	**1**	1.0	8
14			**2**		97
15	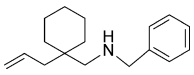	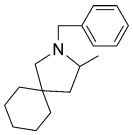	**1**	3.2	9
16			**2**		98
17	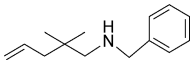	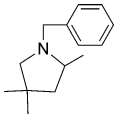	**1**	16	8
18			**2**		96
19	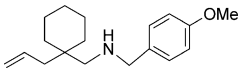	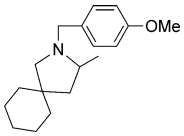	**1**	2.5	2
20			**2**		97

[a] Reaction conditions: amine (20 μL), catalyst (5 mol%), and activator $[PhNMe_2H][B(C_6F_5)_4]$ (5 mol%) in C_6D_6 (0.6 mL) at 80°C. [b] Determined by ^1H NMR spectroscopy against an internal standard. [c] Yield of isolated product after purification. [d] Reaction carried out by heating the NMR probe.

mixture. The secondary aminoalkene that contains a thiophene moiety shows a higher reaction rate than the corresponding aminoalkene with a furan moiety (Table 2, entries 8 and 10). This increase may be attributed to a more effective chelation of the zinc catalyst with the aminofuran moiety. Secondary aminoalkene substituents, those that have either a halogen group or a methoxy group at the *para* position of the phenyl ring, survived under the reaction conditions (Table 2, entries 2 and 6). Again, the catalytic activity of catalyst **2** was remarkably higher than that of catalyst **1**; a similar observation was also noted in the case of the activation of primary aminoalkenes (Table 1). Complex **2** showed comparable activity to that of a previously reported organozinc complex in the presence of an externally added activator.[6l,o]

Kinetic studies of hydroamination reactions: We carried out detailed kinetic studies to gain further insight into the cyclization of primary and secondary aminoalkenes catalyzed by complex **2** in C_6D_6. Kinetic studies of the representative cyclization of primary (see the Supporting Information) and secondary aminoalkenes were carried out by using equimolar amounts of catalyst **2** and $[PhNMe_2H][B(C_6F_5)_4]$. The evolution of the specific resonances of the heterocyclic products was monitored by ^1H NMR spectroscopy relative to an internal standard over the course of the first 7 h and 2.5 h for cyclization of primary and secondary aminoalkenes, respectively.

We carried out detailed kinetic studies for the cyclization of secondary aminoalkene benzyl(2,2-diphenyl-4-pentenyl)-amine (**5**) into its corresponding cyclized product (**6**) with catalyst **2** by using an equimolar amount of $[PhNMe_2H]$-$[B(C_6F_5)_4]$ (with respect to the catalyst) in C_6D_6 at 80°C. To check the order of the reaction for the cyclization of compound **5**, we carried out the reaction with 2.69 mM of complex **2** and 53.97 mM of compound **5**. A plot of $\ln(C/C_0)$ versus time provided a straight line with a negative slope (Figure 3a), thus revealing a pseudo-first-order rate for the cyclization process. To determine the order of the reaction

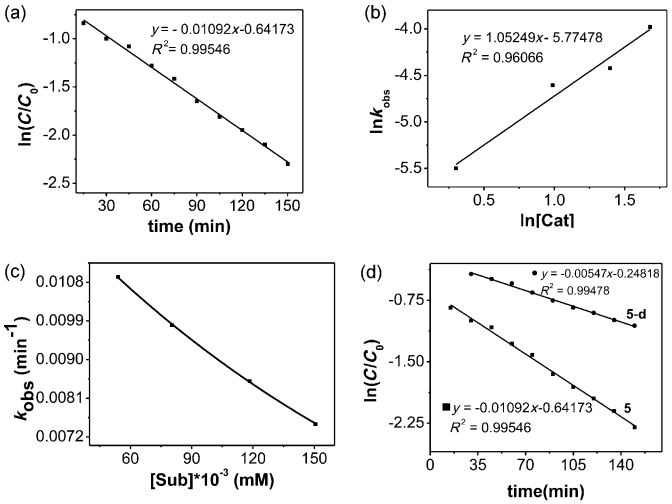

Figure 3. Kinetic studies on the cyclization of a secondary aminoalkene monitored by ^1H NMR spectroscopy (C_6D_6): a) pseudo-first-order plot of the cyclization of compound **5**; b) van't Hoff plot for the cyclization of compound **5** catalyzed by complex **2**; c) plot of k_{obs} versus [Sub] for the cyclization of compound **5**; and d) H/D KIE for the cyclization of compounds **5** and [D]-**5**.

with respect to the catalyst, we carried out the cyclization of compound **5** with various concentrations of complex **2** (1.35 to 5.40 mM) whilst keeping the concentration of substrate **5** fixed (53.97 mM). A plot of k_{obs} versus the concentration of the catalyst revealed a linear increase in the reaction rate with catalyst concentration, thereby confirming a first-order dependency with respect to the catalyst concentration (see the Supporting Information). This result was further confirmed by the van't Hoff plot (Figure 3b). A plot of $\ln k_{obs}$ versus ln[Cat] provided a linear graph (Figure 3b) and the value of the slope was 1.05 (slope = order of the reaction).[13] We also examined the order of the reaction with respect to substrate **5** by keeping the concentration of complex **2** fixed (2.67 mM) and varying the concentration of substrate **5** from 53.97 mM to 150.63 mM (Figure 3c). We found a decrease in the reaction rate with increasing initial concentration of compound **5**, thus indicating an inverse-order dependence on the substrate concentration; a similar observation was also made in the process of cyclization of the primary aminoalkene with catalyst **2** (see the Supporting Information).

Next, the kinetic isotope effect (KIE) for the cyclization process was investigated to gain further insight into the hydroamination reaction. The determination of the KIE is a very useful mechanistic tool that has already been applied to organometallic systems.[14] H/D KIE experiments were carried out under identical reaction conditions, by using compounds **5** and [D]-**5** with 5 mol% of catalyst **2** and 5 mol% of $[PhNMe_2H][B(C_6F_5)_4]$ (Scheme 3). The first-order plots of the cyclization reactions of compounds **5** and [D]-**5** in C_6D_6 at 80°C indicate that $k_{obs} = 0.01092\ min^{-1}$ and $k_{obs} = 0.00547\ min^{-1}$, respectively, which translate into a KIE of 2.0 (Figure 3d). This observation suggests that hydrogen, which is derived from the NH group of compound **5**, is involved in one of the key steps of the cyclization process, similar to that observed for the cyclization of the primary aminoalkene with catalyst **2** (see the Supporting Information).

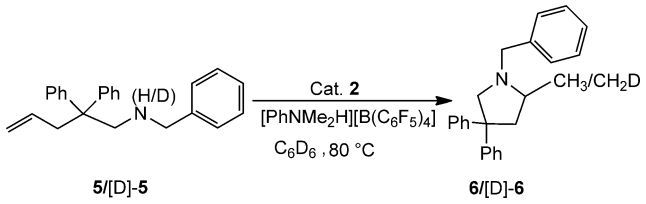

Scheme 3. Catalytic reaction of complex **2** with benzyl(2,2-diphenyl-4-pentenyl)amine (**5**) and benzyl(2,2-diphenyl-4-pentenyl)amine-*d* ([D]-**5**) in C_6D_6 at 80°C.

Activation parameters for the cyclization of compound 5: To obtain the activation parameters for the cyclization of compound **5** by using catalyst **2** in C_6D_6, a series of reactions was carried out over a range of temperatures (50–80°C). In each case, a first-order rate constant was obtained from the plots of $\ln(C/C_0)$ versus time over this temperature range. Eyring analysis for the cyclization of compound **5** afforded $\Delta H^{\neq} = 11.3\ kcal\,mol^{-1}$ and $\Delta S^{\neq} = -35.75\ cal\,K^{-1}\,mol^{-1}$ (Figure 4a), whereas Arrhenius analysis afforded $E_a = 11.68$ kcal mol^{-1} (Figure 4b).

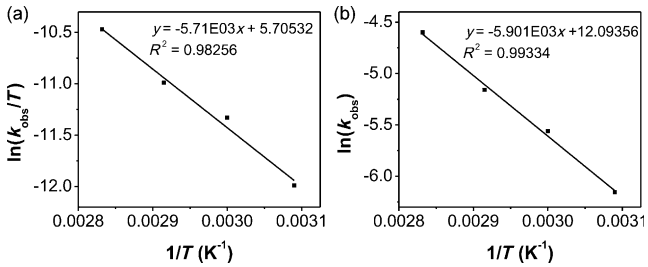

Figure 4. a) Eyring plot for the cyclization of compound **5** catalyzed by complex **2** in C_6D_6 over the temperature range 50–80°C with the following concentrations: [Sub] = 53.97 mM, [Cat] = 2.67 mM; b) Arrhenius plot for the cyclization of compound **5** catalyzed by complex **2** in C_6D_6 over the temperature range 50–80°C with the following concentrations: [Sub] = 53.97 mM, [Cat] = 2.67 mM.

In summary, the kinetic analyses of the cyclization of compounds **3** and **5** catalyzed by complex **2** revealed that both cyclization processes of primary and secondary aminoalkenes follow similar kinetics with overall pseudo-first-order reaction rates. The reaction rates exhibit first-order dependence on the concentration of the catalyst and inverse-order dependence with respect to the concentration of the substrates. The KIE study on primary and secondary aminoalkenes suggests that the N–H bond plays a key role in the cyclization process, that is, it is involved in one of the rate-limiting steps in the catalytic cycle.

Mechanistic investigation—combined NMR and computational studies: Previous studies have demonstrated that, in the presence of $[PhNMe_2H][B(C_6F_5)_4]$ as an activator, organozinc complexes exhibit good catalytic activity for primary and secondary aminoalkenes.[6a–c,n,o] The activator abstracts the methyl group that is attached to the zinc center to generate a zinc cation in situ, which functions as the catalytically active species. The addition of an activator to the organozinc complex greatly enhances its catalytic activity,[6a–c,n,o] which is superior to the catalytic activity of the activator alone.[15] Herein, the results of the catalytic intramolecular hydroamination of primary and secondary aminoalkenes reveal that catalyst **2** has a remarkably higher reactivity than that of catalyst **1** under identical reaction conditions (Tables 1 and 2). To understand this notable difference in catalytic activity and to understand the mechanistic pathway for the cyclization process, we carried out an in situ NMR study, as well as a detailed computational study. The in situ NMR experiments revealed that, after the addition of the activator in equimolar amounts (Scheme 4), the ZnMe resonance in complex **2** ($\delta = 0.04$ ppm) vanishes completely and resonances at $\delta = 0.15$ and 2.5 ppm appear that are due to the generation of CH_4[16] and $PhNMe_2$, respectively, thus

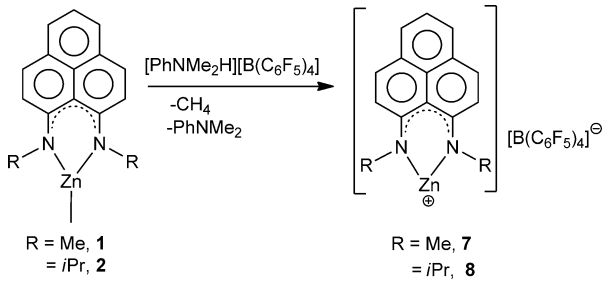

Scheme 4. Synthesis of the zinc-centered cations **7** and **8**.

confirming the role of the activator as a methyl abstractor and the generation of a zinc cation (Figure 5). Previously, Roesky and co-workers demonstrated that the use of an equimolar activator with respect to the methylzinc complex generated a zinc cation in situ, which, in turn, facilitated the intramolecular hydroamination reactions of unactivated aminoalkenes.[6b] Earlier, Bochmann and co-workers isolated a similar type of zinc cation from its corresponding zinc–alkyl complex by using a boron-based Lewis acceptor.[17]

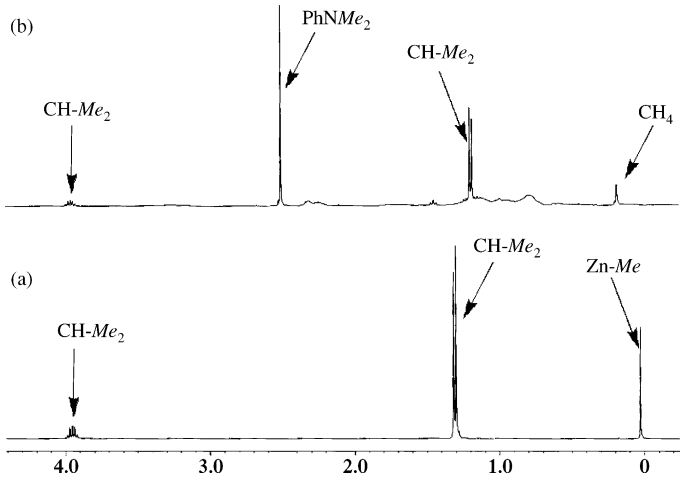

Figure 5. ^{1}H NMR spectra of a) [*N*(*i*Pr),*N*(*i*Pr)-PLY]ZnMe (**2**) and b) [*N*(*i*Pr),*N*(*i*Pr)-PLY]ZnMe with $[PhNMe_2H][B(C_6F_5)_4]$ in C_6D_6, which reveal the absence of the ZnMe resonance and the appearance of CH_4 and $PhNMe_2$ resonances.

To understand the difference in catalytic activity between complexes **1** and **2** for the hydroamination reaction, we carried out a computational study on complexes **1** and **2**, as well as on their corresponding cations (**7** and **8**, Scheme 4), which were generated after the addition of an equimolar amount of the activator to solutions of complexes **1** and **2**, respectively. The change in Gibbs free energy (ΔG) for the formation of zinc-centered cations **7** and **8** are calculated as -2.4 and -21.6 kcal mol^{-1}, respectively. This result indicates that the formation of cation **8** is more-favored than that of cation **7**. The frontier orbitals (HOMO and LUMO of cations **7** and **8**), as ascertained by DFT calculations, are shown in Figure 6. The LUMOs of cations **7** and **8** clearly indicate that they are primarily zinc-centered. Furthermore, the computed HOMO–LUMO energy gap of zinc-centered cations **7** and **8** are 64.6 and 70.6 kcal mol^{-1}, respectively, thus supporting a higher stability of cation **8** over that of cation **7** (see the Supporting Information).[18]

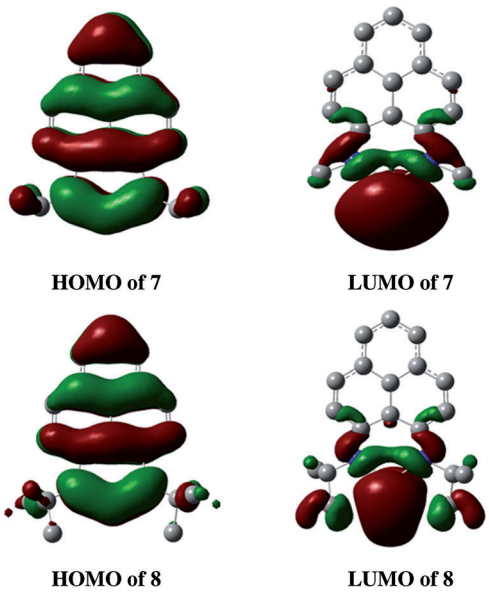

Figure 6. Computed HOMOs and LUMOs of the zinc-centered cations of compounds **7** and **8**.

To further understand the stability of the catalytically active cation, we investigated the activity of in-situ-generated cation **8** in successive catalytic cycles. One of the major problems in homogeneous catalysis is the inability to recycle the catalysts because they are inseparable from the reaction mixture. Herein, we monitor the longevity of catalyst **2** by performing several catalytic runs within the same reaction vessel to test whether the catalyst remained live over several catalytic cycles.[19] Four successive catalytic runs were carried out by using 5 mol% of catalyst **2** and equimolar amounts of $[PhNMe_2H][B(C_6F_5)_4]$ and secondary aminoalkene substrate **5** with respect to an internal standard (hexamethyl benzene) in C_6D_6 at 80 °C by using an in situ recycling procedure. After complete consumption of the substrate, a fresh batch of substrate was introduced without introducing any additional catalyst. After each 4 h interval, the conversion into the product was checked by recording a ^{1}H NMR spectrum of the reaction mixture. The catalytic runs were repeated for four successive cycles. We found that catalyst **2** remained catalytically active in up to four consecutive runs (Figure 7); however, a gradual decrease in the activity was noted after each 4 h interval by NMR spectroscopy. Nevertheless, this result clearly indicates that the catalytically active species remains live for several consecutive runs of the catalytic cycles.

Although there have been several reports on hydroamination reactions with zinc catalysts in recent years,[6] there have not been any reports on the mechanistic pathways for zinc-catalyzed hydroamination reactions. The plausible mechanistic pathways[6b,o] for the zinc-catalyzed hydroamina-

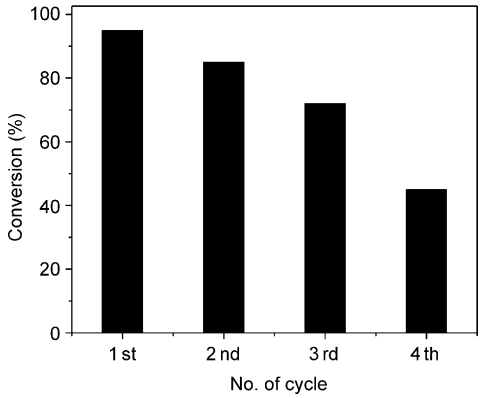

Figure 7. Catalyst-longevity test for the cyclization of compound **5** with catalyst **2** in C_6D_6 at 80 °C.

tion reaction may involve either activation of the C=C double bond (also known as alkene activation) or activation of the N–H single bond (also known as amine activation, Scheme 5).[6b] Earlier studies have reported that hydroamination with catalysts of rare-earth metals, early transition metals, and Group 2 metals proceed through the amine-activation pathway,[1g,2d,4a,d] whilst late-transition-metal-based catalysts follow the alkene-activation pathway.[4k,o] Thus, in this case, zinc catalysts **1** and **2** may follow either the activation of the C=C bond (alkene activation; Scheme 5, left)[20] or the activation of the N–H bond (amine activation; Scheme 5, right).[21]

Given the lack of spectroscopic evidence of the catalytic reaction mixture at various temperatures, which would enable the definite identification of catalytic intermediates and to gain further insight into the details of the mechanism of the zinc-catalyzed hydroamination reaction, despite our several attempts by using NMR spectroscopy, this process was subjected to computational examination. To corroborate the kinetic data and to gain further insight into the nature of the intermediates in the catalytic cycle, we carried out detailed density functional theory (DFT) calculations to investigate the mechanism of the intramolecular hydroamination of a model substrate (**5**). During these calculations, no structural simplification of any of the key species was imposed and the data reported herein are focused exclusively on the most-accessible pathways. DFT calculations have previously been utilized for unraveling the mechanistic cycle of the hydroamination reaction by several groups by using different metal catalysts.[22]

The calculations were started by examining the possibility of different ligation modes of the aminoalkene substrate (**5**) to coordinatively unsaturated zinc-centered cation **8**, which was generated from complex **2** (Figure 8). In principle, the substrate can attach to the zinc center in different ways: through a chelating aminoalkene (**AA**), a bis-hapto association to the zinc center through its olefinic bond (**A**), or through its amine functionality (**A1**). The changes in the computed Gibbs free energy (ΔG) for the formation of structures **A** and **A1** are uphill by 2.1 and 3.8 kcal mol^{-1}, respectively, relative to that of **AA**. This subtle difference in ΔG indicates the possibility of these species existing in rapid equilibrium. Species **A** and **A1** were used as starting points for the alkene- and amine-activation cycles, respectively, and the **AA** species is referred to as the catalyst in its resting state,[4k] from which **A** or **A1** can be generated.

Catalytic hydroamination through activation of the C=C bond (alkene activation): The catalytic hydroamination of secondary aminoalkenes by the alkene-activation pathway includes (Scheme 5, left): 1) coordination of the olefin moiety to the metal center; 2) nucleophilic attack of the amine on the olefin moiety that is preactivated by the co-

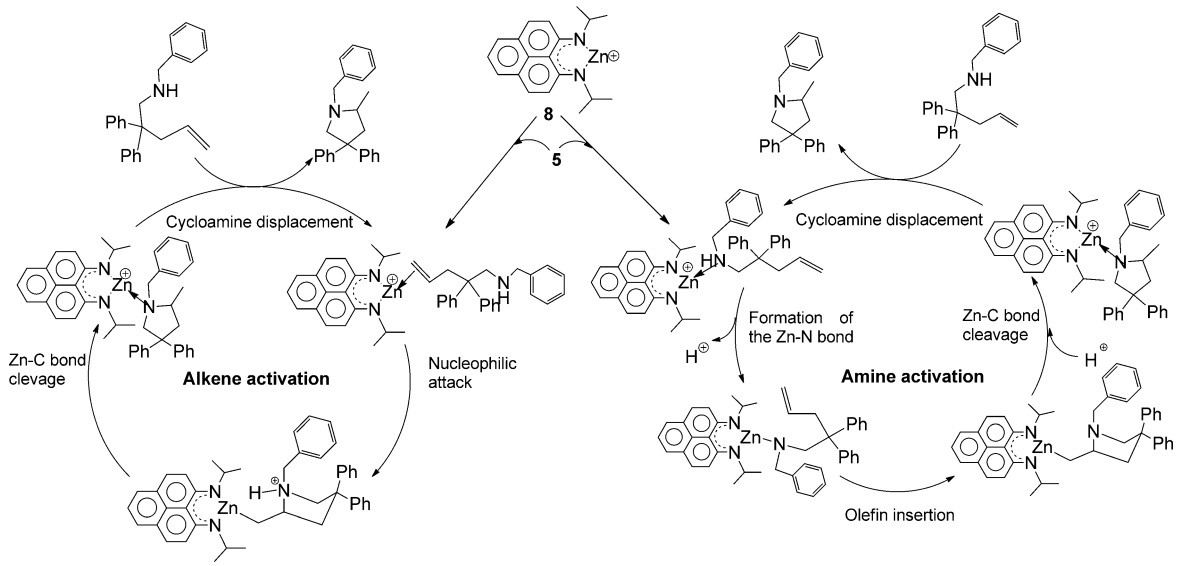

Scheme 5. Plausible mechanistic pathways for the intramolecular hydroamination of model substrate **5** by using cation **8**, which was generated from catalyst **2**; counterions are not shown for the sake of clarity.

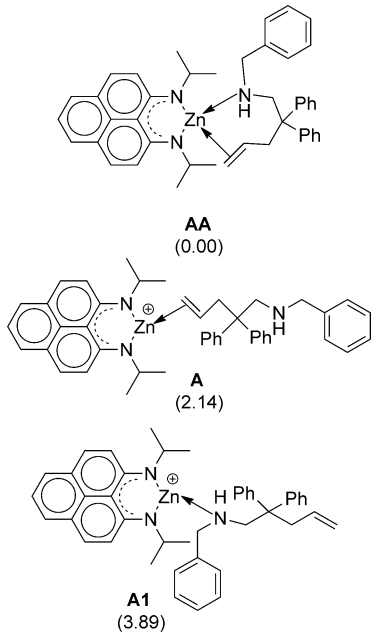

Figure 8. Various forms of the catalytically competent species (computed Gibbs free energy changes in kcal mol^{-1} relative to **AA** are given in parentheses); counterions are not shown for the sake of clarity.

ordination to the metal center; 3) protonolysis of the Zn–alkyl bond; and 4) displacement of the cyclic pyrrolidine by a new substrate molecule to regenerate the active catalyst (**A** in this case). Detailed calculations were carried out with substrate **5** by using cation **8**. The Gibb's free energy profile, which considers the most-accessible reaction pathway for the intramolecular hydroamination reaction, is shown in Figure 9. Initially, the aminoalkene (**5**) attaches onto the zinc-centered cation (**8**) to generate the Zn–phenalenyl intermediate (**A**), which can exist in rapid equilibrium with the catalyst-resting state (**AA**) that contains a chelating aminoalkene. Although **AA** represents the most-stable form, it can be easily converted into **A**, which is uphill by only 2.1 kcal mol^{-1}. Then, the reaction proceeds through the attack of the amine functionality on the olefin unit of **A** (Figure 9) to produce intermediate **B**. Transformation of **A** into **B** proceeds through the TS [**A**-**B**] transition state, which lies 21.5 kcal mol^{-1} higher in energy than **A**.

Intermediate **B** carries the hydrogen atom on the quaternized ammonium center, which undergoes a proton transfer from the ammonium unit to the carbon atom that is attached to the zinc center. Cleavage of the Zn–C bond leads to the formation of intermediate **C**. In the most-accessible pathway that commences from intermediate **B**, the ammoni-

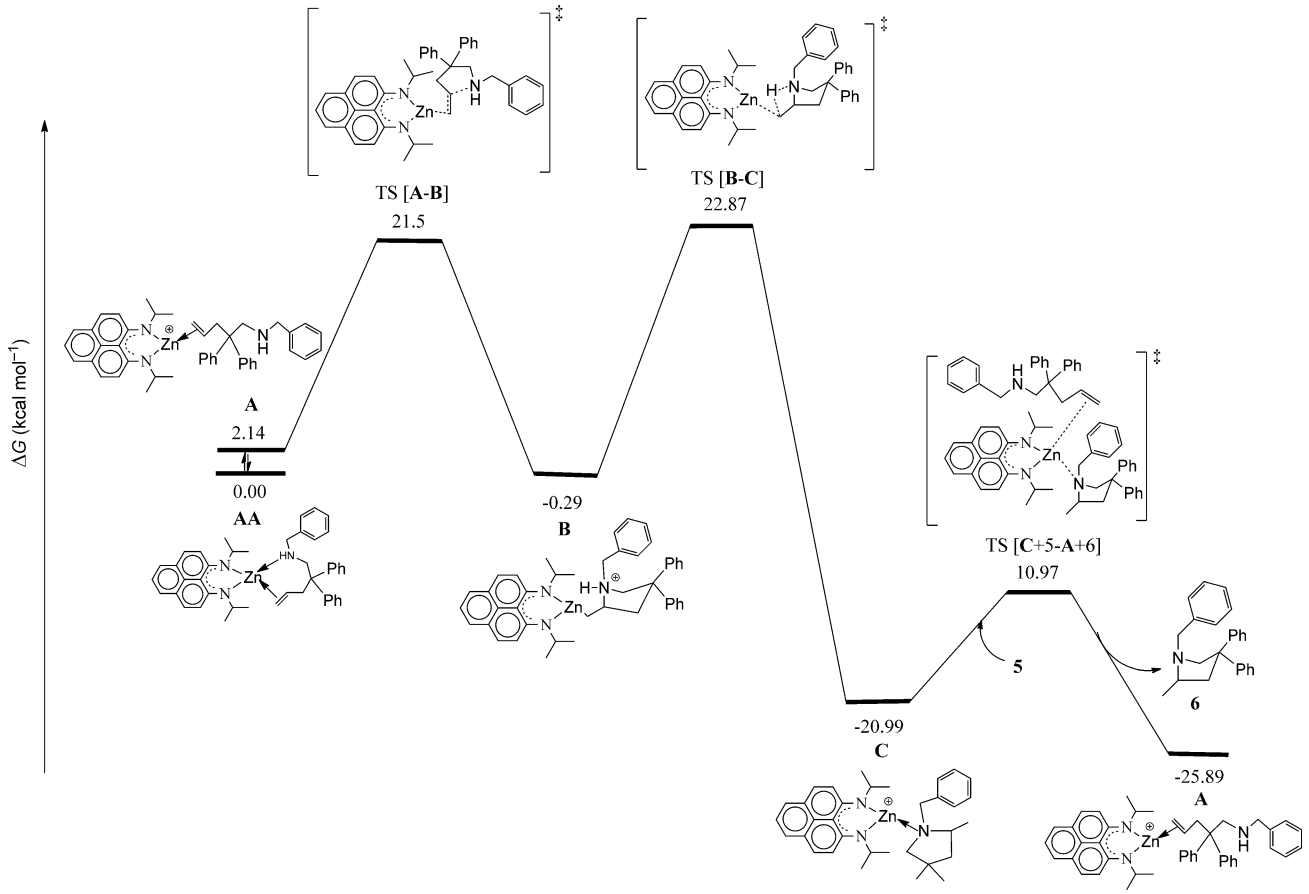

Figure 9. Free-energy profile for the intramolecular hydroamination of compound **5** by catalyst **8** through an alkene-activation pathway. Only the most-accessible steps are shown; counterions are not shown for the sake of clarity.

um unit is suitably oriented toward the zinc center, such that its deprotonation does not cause major structural reorganization (TS [**B**-**C**], Figure 9). Transformation from **B** into **C** proceeds through TS [**B**-**C**], which involves an energy barrier of 22.8 kcal mol^{-1}. Thereafter, the incoming substrate displaces the desired pyrrolidine product (**6**) from intermediate **C** and regenerates the catalytically active species (**A**), which again participates in the catalytic cycle. Transformation of intermediate **C** into catalytically active species **A** involves a transition state that constitutes the zinc complex, substrate (**5**), and cyclic pyrrolidine **6** (TS [**C+5 A+6**]). The transformation from **C** into **A** involves an energy barrier of 10.9 kcal mol^{-1}. Transformation from **B** into **C** involves the highest uphill energy (22.8 kcal mol^{-1}) of the cycle, thus indicating that it is the slowest step in the catalytic process. This transformation, which involves cleavage of the N–H bond, is the rate-determining step of the catalytic cycle, which is in agreement with the data that were obtained from the KIE studies. Figure 10 shows the energy-optimized structures of the key intermediates and the transition states in the catalytic hydroamination of compound **5** catalyzed by cation **8**.

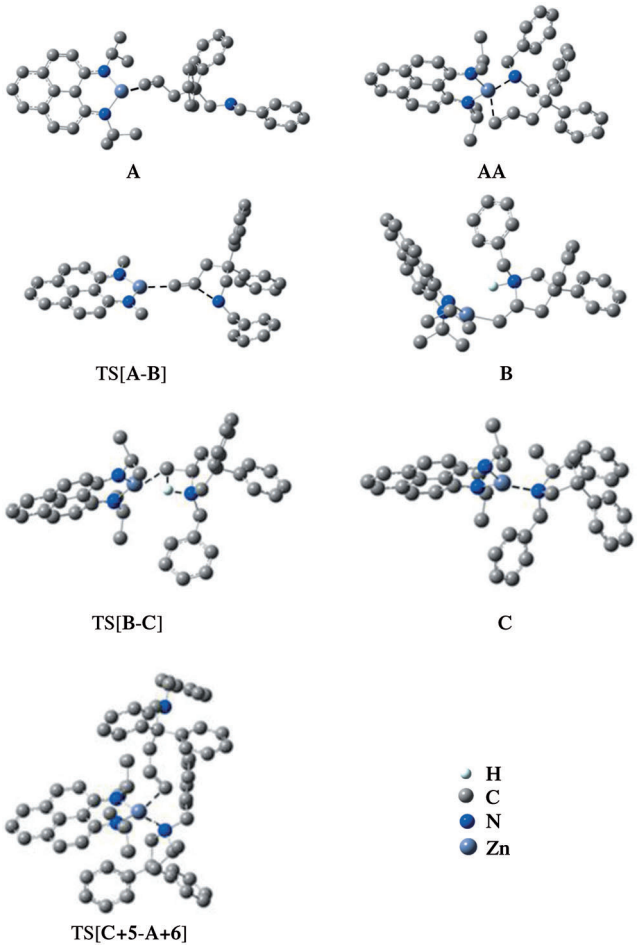

Figure 10. Optimized structures of the key intermediates and transition states for the alkene-activation pathway catalyzed by cation **8**, which was generated from complex **2**; hydrogen atoms (other than **B** and TS [**B**-**C**]) and counterions are not shown for the sake of clarity.

Catalytic hydroamination through activation of the N–H bond (amine activation): An alternative pathway for the catalytic hydroamination of secondary aminoalkenes by amine activation includes (Scheme 5, right): 1) formation of the Zn–N bond, which leads to the zinc–amide complex; 2) insertion of the olefinic unit into the Zn–N bond; and 3) displacement of the cyclic pyrrolidine by a new substrate molecule to regenerate the active catalyst (**A1**). The Gibb's free energy profile for the most-accessible reaction pathway for the intramolecular hydroamination reaction is shown in Figure 11. For the amine-activation process, the first step involves the generation of intermediate **A1** (Figure 8), which can be in rapid equilibrium with catalyst-resting state **AA** (Figure 11) because **A1** is only 3.8 kcal mol^{-1} higher in energy than **AA**. The formation of the Zn–N bond, thereby leading to the initial zinc–amide complex, was postulated to proceed through transition state TS [**A1-B1**] (Figure 11). It is evident from the calculations that the formation of the Zn–N bond is almost insurmountable, with an energy barrier of 44.8 kcal mol^{-1}, thereby making the amine-activation pathway much-less favorable than the alternative alkene-activation pathway; the highest energy barrier is only 22.8 kcal mol^{-1} in the case of the alternative alkene-activation pathway. These values are comparable to those that were calculated recently for the iridium-catalyzed hydroamination reaction by Tobisch, Stradiotto, and co-workers.[4k] Thus, further optimization of other intermediates was not performed for the amine-activation process because, from the first step of the mechanistic cycle, it is evident that the amine-activation pathway involves a much-higher energy barrier than any steps in the alkene-activation pathway, thus indicating that the alkene-activation pathway is preferred. This result may be correlated to the earlier-established fact[23] that the low kinetic basicity of the Zn–C bond, as a consequence of the high covalency with respect to the Zn–N bond, leads to the formation of Zn–C bond being thermodynamically more-preferred over the Zn–N bond. Furthermore, Bochmann and co-workers have earlier isolated and crystallographically characterized an η^2-bound toluene–Zn^{II} complex.[24] Figure 12 shows the energy-optimized structures of the key intermediates and transition state of the catalytic hydroamination of compound **5** catalyzed by compound **8** for the amine-activation pathway.

Once the alkene-activation pathway was established as the preferred pathway, we further performed DFT calculations on the catalytic cycle of the hydroamination reaction catalyzed by cation **7**, which was generated from complex **1**, to understand the observed remarkable difference in catalytic efficiency between catalysts **1** and **2** (Table 1 and Table 2). The Gibb's free energy profile, which considers the most-accessible reaction pathway for the intramolecular hydroamination reaction is shown in Figure 13. This energy profile indicates that, in the case of catalyst **1**, the catalytic pathway from structures **A′** to **C′** involves slightly higher energy barriers than that using catalyst **2**, which supports the lower catalytic activity of complex **1** versus complex **2**. However, this slight difference in the Gibb's free energy profile does not

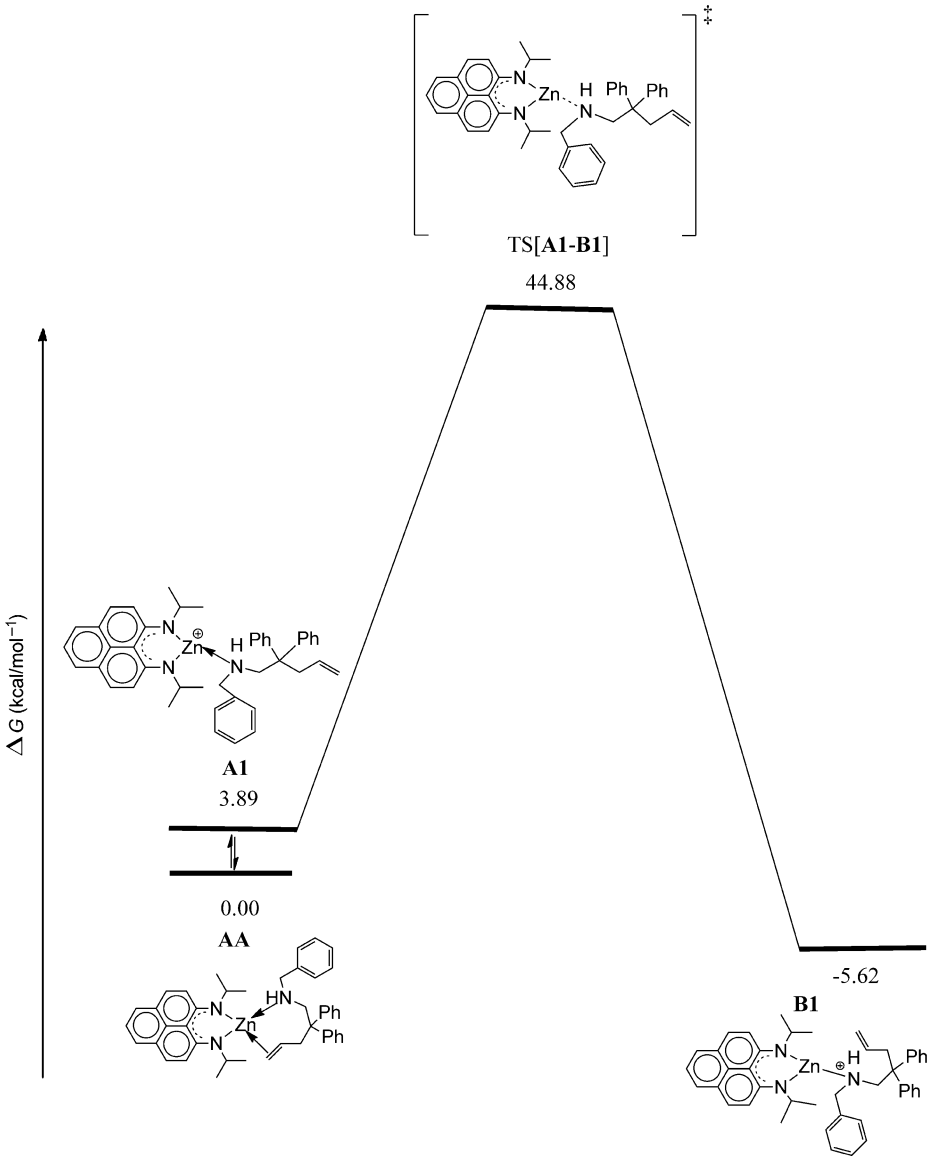

Figure 11. Free-energy profile for the intramolecular hydroamination of compound **5** catalyzed by complex **8** through an amine-activation pathway. Only the most-accessible step is shown; counterions are not shown for the sake of clarity.

adequately explain the origin of the remarkable difference in catalytic activity. It seems more likely that the dramatic difference originates from the higher stability and more-facile formation of cation **8** from complex **2** than that of cation **7** from complex **1**. The energy-optimized structures of the key intermediates and transition states in the catalytic hydroamination of compound **5** catalyzed by compound **7** can be found in the Supporting Information.

Mechanistic conclusions: Thus, from this investigation, we arrive at the following mechanistic conclusions (Scheme 6): 1) the zinc-catalyzed hydroamination reaction preferably follows the alkene-activation pathway rather than the alternative amine-activation pathway; 2) the first step of alkene activation involves coordination of the alkene moiety to the electrophilic zinc center, thereby forming intermediate **A**. In turn, intermediate **A** can exist in rapid equilibrium with the catalyst-resting state (**AA**) having the chelating mode of aminoalkene coordination; 3) the activated alkene moiety in intermediate **A** is then attacked by the nucleophilic nitrogen atom of the amino group, thus leading to the formation of intermediate **B**; 4) proton transfer from the ammonium unit in structure **B** onto the carbon atom that is attached to the Zn center leads to the cleavage of the Zn–C bond and generates intermediate **C**, which proceeds through TS [**B**-**C**]; and 5) displacement of the cycloamine by the incoming substrate occurs and regenerates the catalytically active species (**A**).

Conclusion

We have prepared and characterized two organozinc complexes that contain symmetrical phenalenyl (PLY)-based N,N-ligands. These organozinc complexes were used as catalysts for hydroamination reactions. A combined approach that involved NMR experiments and DFT calculations was adopted to unravel the mechanistic pathway for the zinc-catalyzed hydroamination reaction. The reactions of phenalenyl-based ligands with $ZnMe_2$ led to the formation of organozinc complexes [*N*(Me),*N*(Me)-PLY]-ZnMe (**1**) and [*N*(*i*Pr),*N*(*i*Pr)-PLY]ZnMe (**2**) under the evolution of methane. The solid-state structures of complexes **1** and **2** were determined by single-crystal X-ray crystallography. Complexes **1** and **2** were used as catalysts for the intramolecular hydroamination of unactivated primary and secondary aminoalkenes. Complex **2** exhibited a catalytic activity that was remarkably higher than that of complex **1** under identical reaction conditions. Detailed NMR spectroscopic studies and DFT calculations were utilized to understand the mechanistic cycle of the zinc-catalyzed hydroamination reaction. In situ NMR experiments supported the formation of a catalytically active zinc cation and the DFT calculations showed that the more-active catalyst (**2**) gener-

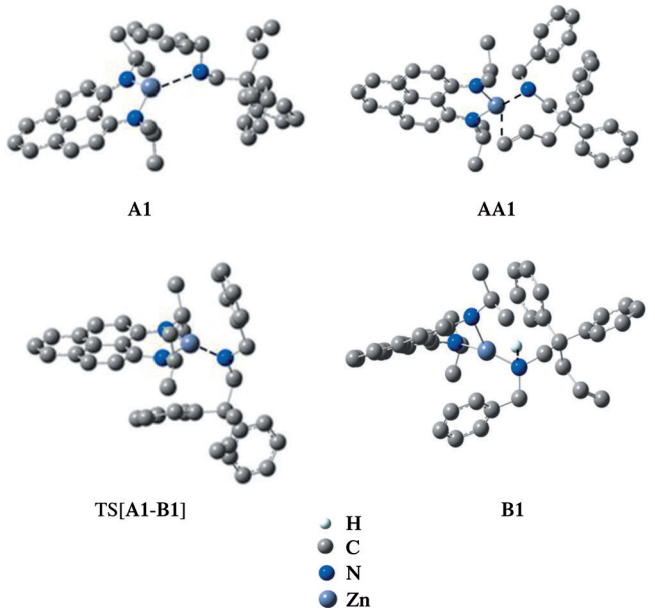

Figure 12. Optimized structures of the key intermediates and transition state for the amine-activation pathway catalyzed by compound **8**; hydrogen atoms (except in **B1**) and counterions are not shown for the sake of clarity.

ated a stable cation. The stability of the catalytically active cation was further supported by the in situ recycling procedure, which confirmed the persistent nature of the cation for successive hydroamination cycles. Kinetic studies of the cyclization of both primary and secondary aminoalkenes catalyzed by complex **2** revealed that both cyclization processes followed similar reaction kinetics with pseudo-first-order reaction rates. KIE studies on primary and secondary aminoalkenes suggested that the cleavage of the N–H bond in both primary and secondary aminoalkenes plays a key role in the cyclization process. The DFT calculations showed, for the first time, that the preferred pathway for the zinc-catalyzed hydroamination reaction involves alkene activation rather than amine activation. A detailed investigation with DFT calculations supported the conclusion that the remarkably higher catalytic efficiency originates from the higher stability and more-facile formation of the zinc-centered cation from complex **2** than from complex **1**.

Experimental Section

All manipulations were performed under a dry nitrogen atmosphere by using standard Schlenk techniques or inside an MBraun glovebox that was maintained at or below a level of 0.1 ppm O_2 and H_2O with oven-

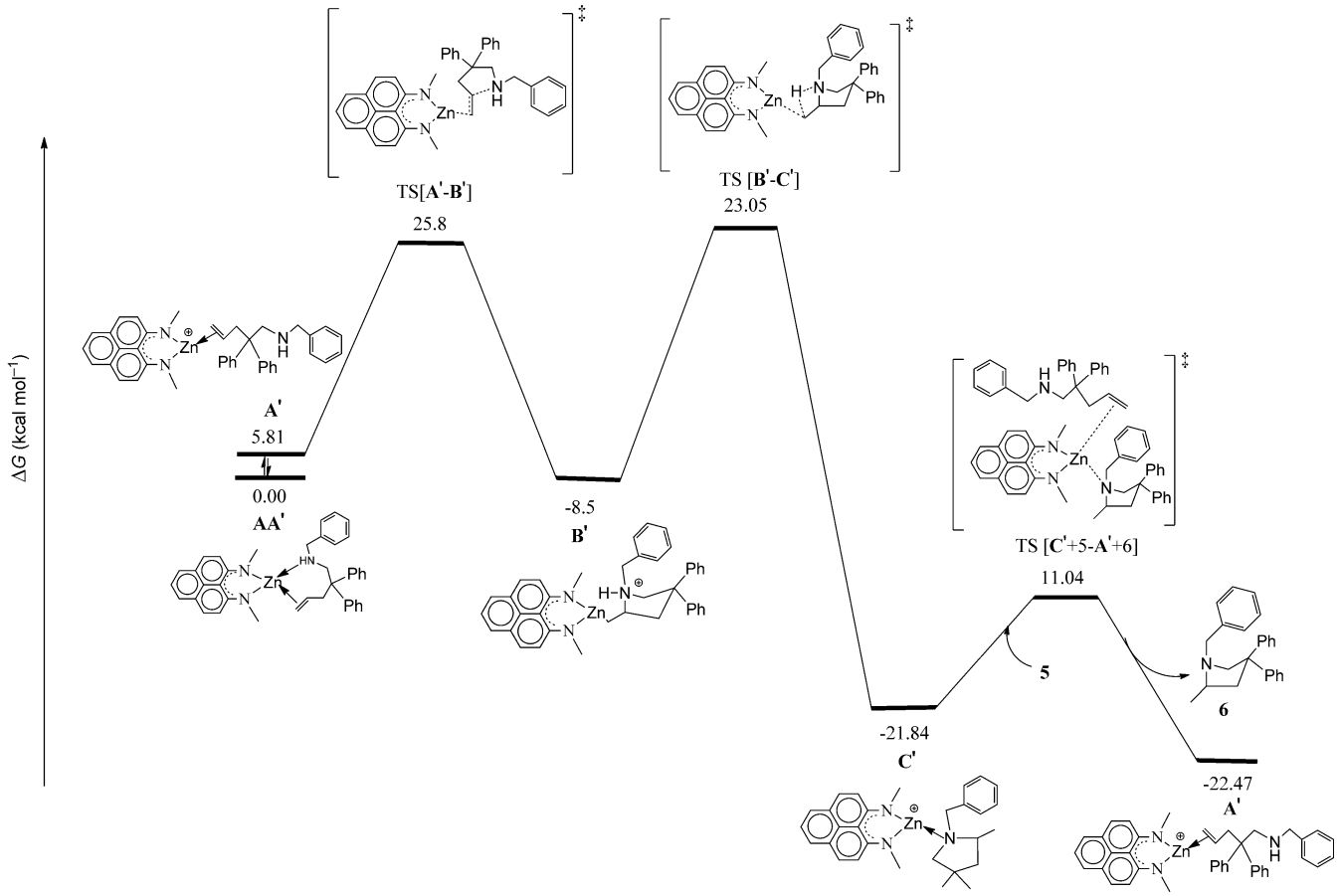

Figure 13. Free-energy profile for the intramolecular hydroamination of compound **5** catalyzed by compound **7** through an alkene-activation pathway. Only the most accessible steps are shown; counterions are not shown for the sake of clarity.

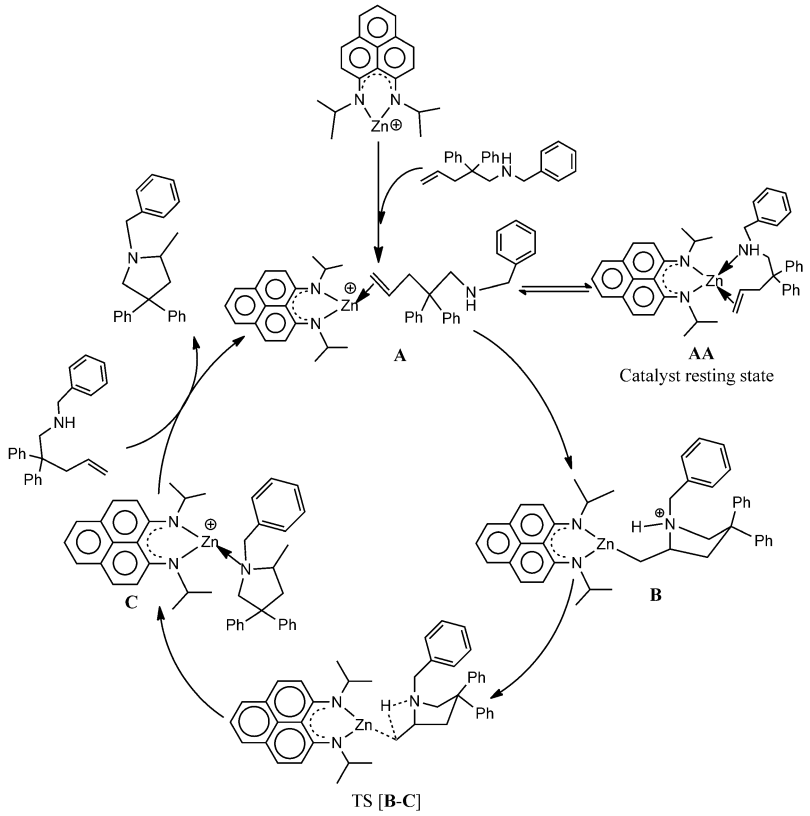

Scheme 6. Proposed mechanism for the intramolecular hydroamination of aminoalkenes catalyzed by cation **8**, which was generated from complex **2**; counterions are not shown for the sake of clarity.

dried glassware (130 °C) that was evacuated whilst hot prior to use. All solvents were distilled from Na/benzophenone prior to use. Other chemicals were purchased commercially and used as received. Deuterated benzene was purchased from Cambridge Isotope Laboratories, dried with a sodium/potassium alloy, stored over 4 Å molecular sieves prior to use. ^{1}H and ^{13}C NMR spectra were recorded on a JEOL-ECS 400 MHz spectrometer with C_6D_6 as the solvent. The following abbreviations are used to describe the peak patterns, when appropriate: s (singlet), d (doublet), t (triplet), m (multiplet), and br (broad). Elemental analysis was performed by the Analytisches Labor des Instituts für Anorganische Chemie der Universität Göttingen. Melting points were measured in sealed glass tubes on a Büchi melting point B540 instrument and are uncorrected.

Starting materials: 9-*N*-Methylamino-1-*N*′-methylimino-phenalene[8d] and 9-*N*-isopropylamino-1-*N*′-isoproylimino-phenalene[10b] were synthesized according to literature procedures. Dimethyl zinc (1.2 M in toluene) and [PhNMe$_2$H][B(C$_6$F$_5$)$_4$] were purchased from Acros Organics. Aminoalkenes were prepared from commercially available starting materials (Aldrich, Acros Organics, and Fluka). Aminoalkene substrates 2,2-diphenylpent-4-en-1-amine,[4m] (1-allylcyclohexyl)methylamine,[25a] 2,2-dimethylhex-5-enylamine,[3e] 4-methyl-2,2-diphenylpent-4-en-1-amine,[25b] 4-methyl(1-allylcyclohexyl)methylamine,[25b] benzyl(2,2-diphenyl-4-pentenyl)amine,[4m] (4-bromobenzyl)(2,2-diphenyl-4-pentenyl)amine,[4m] (4-methoxybenzyl)(2,2-diphenyl-4-pentenyl)amine,[25c] (2,2-diphenylpent-4-enyl)furan-2-ylmethylamine,[6b] (2,2-diphenylpent-4-enyl)thiophen-2-ylmethylamine,[6b] (1-allylcyclohexylmethyl)benzylamine,[4m] (1-allylcyclohexylmethyl)(4-bromobenzyl)amine,[25d] 2-furan-2-ylmethyl-3-methyl-2-azaspiro[4.5]decanamine,[6o] (1-allylcyclohexylmethyl)(4-methoxybenzyl)amine,[25d] and benzyl(2,2-dimethyl-4-pentenyl)amine[4m] were prepared according to literature procedures and dried by distilling twice from CaH_2. The hydroamination products are known compounds and were identified by comparison with their literature NMR spectroscopic data.[3c,6b,o,25]

Synthesis of [*N*(Me),*N*(Me)-PLY]ZnMe (1): A solution of [H*N*(Me),*N*(Me)-PLY] (0.222 g, 1.0 mmol) in toluene (25 mL) was added dropwise to a solution of $ZnMe_2$ (1.0 mL, 1.2 mmol, 1.2 M in toluene) in toluene (20 mL) at −78 °C. The reaction mixture was slowly warmed to ambient temperature and stirred at 25 °C for 3 h. The resulting red solution was then concentrated to approximately 30 mL under reduced pressure and kept at 0 °C. After 1 day, deep-red crystals of the title compound developed in the reaction mixture. Yield: 0.250 g (82 %); m.p. 200–202 °C; ^{1}H NMR (C_6D_6, 400 MHz, 298 K): δ = 7.64 (d, J = 7.3 Hz, 2H; Ar*H*), 7.54 (d, J = 9.7 Hz, 2H; Ar*H*), 7.24 (t, J = 7.3 Hz, 1H; Ar*H*), 7.10 (d, J = 9.1 Hz, 2H; Ar*H*), 3.15 (s, 6H; N*Me*$_2$), −0.20 ppm (s, 3H; Zn*Me*); ^{13}C NMR (C_6D_6, 100 MHz, 298 K): δ = 162.1, 135.2, 130.7, 129.8, 125.6, 120.5, 117.8, 109.1, 40.0, −4.3 ppm; elemental analysis calcd (%) for $C_{16}H_{16}N_2Zn$: C 63.70, H 5.35, N 9.29; found: C 63.53, H 5.73, N 9.32.

Synthesis of [*N*(*i*Pr),*N*(*i*Pr)-PLY]-ZnMe (2): A solution of [H*N*(*i*Pr),*N*-(*i*Pr)-PLY] (0.278 g, 1.0 mmol) in toluene (25 mL) was added dropwise to a solution of $ZnMe_2$ (1.0 mL, 1.2 mmol, 1.2 M in toluene) in toluene (20 mL) at −78 °C. The reaction mixture was slowly warmed to ambient temperature and then heated at 110 °C for 24 h. The resulting deep-red solution was then concentrated to approximately 10 mL under reduced pressure and kept at 25 °C inside a glovebox. After a few days, red crystals of the title compound developed in the reaction mixture by using the slow-solvent-evaporation technique. Yield: 0.280 g (78 %); m.p. 143–145 °C; ^{1}H NMR (C_6D_6, 400 MHz, 298 K): δ = 7.59 (d, J = 7.3 Hz, 2H; Ar*H*), 7.48 (d, J = 9.1 Hz, 2H; Ar*H*), 7.22 (t, J = 7.3 Hz, 1H; Ar*H*), 7.16 (d, partially obscured by C_6D_6, J = 9.7 Hz, 2H; Ar*H*), 3.99–3.96 (m, 2H; NC*H*Me$_2$), 1.34 (d, J = 6.7 Hz, 12H; CH*Me*$_2$), 0.04 ppm (s, 3H; Zn*Me*); ^{13}C NMR (C_6D_6, 100 MHz, 298 K): δ = 160.4, 135.2, 130.2, 129.3, 125.6, 120.3, 118.7, 108.7, 51.1, 25.0, −5.9 ppm; elemental analysis calcd (%) for $C_{20}H_{24}N_2Zn$: C 67.23, H 6.72, N 7.84; found: C 66.84, H 6.31, N 7.55.

General procedure for the intramolecular hydroamination of primary aminoalkenes: All of the reactions were performed in an NMR tube in a N_2-filled glovebox. A pre-dried NMR tube was charged with the aminoalkene (20 μL) and a solution of the catalyst (5 mol %), [PhNMe$_2$H][B(C$_6$F$_5$)$_4$] (5 mol %), and hexamethyl benzene (as an internal standard) in C_6D_6 (0.6 mL) was added under a nitrogen atmosphere. The NMR tube was sealed and the reaction mixture was heated in a preheated oil bath that was maintained at 120 °C for the stated time. The reaction progress was monitored by ^{1}H NMR spectroscopy. Yields were determined by comparing the integration of the internal standard with a well-resolved signal for the heterocyclic product. Purification: 2-methyl-4,4-diphenyl pyrrolidine (cyclized product of Table 1, entry 2) was purified by column chromatography on silica gel (CH_2Cl_2/MeOH, 10:1); yield of isolated product: 90 %.

General procedure for the intramolecular hydroamination of secondary aminoalkenes: All of the reactions were performed in an NMR tube in a N_2-filled glovebox. A pre-dried NMR tube was charged with the aminoalkene (20 μL) and a solution of the catalyst (5 mol %), [PhNMe$_2$H][B(C$_6$F$_5$)$_4$] (5 mol %), and hexamethyl benzene (as an internal standard) in

C_6D_6 (0.6 mL) was added under a nitrogen atmosphere. The NMR tube was sealed and the reaction mixture was heated at 80 °C in a pre-heated oil bath for the stated time. The reaction progress was monitored by ^{1}H NMR spectroscopy. Yields were determined by comparing the integration of the internal standard with a well-resolved signal for the heterocyclic product. Purification: 1-(4-bromobenzyl)-2-methyl-4,4-diphenylpyrrolidine (cyclized product of Table 2, entry 2) was purified by column chromatography on silica gel (*n*-hexane/EtOAc, 9:1); yield of isolated product: 92%.

Catalyst longevity test for intramolecular hydroamination reaction of compound 5: The catalyst-longevity experiment was carried out inside a N_2-filled glovebox. A pre-dried NMR tube was charged with the aminoalkene (20 μmol) and a solution of the catalyst (5 mol%), $[PhNMe_2H][B(C_6F_5)_4]$ (5 mol%), and hexamethyl benzene (as an internal standard, 1 equiv with respect to the substrate) in C_6D_6 (0.6 mL) was added under a nitrogen atmosphere. The NMR tube was sealed and the reaction mixture was heated at 80 °C for 4 h. The reaction was monitored by ^{1}H NMR spectroscopy after 4 h. Conversion was determined by comparing the integration of a well-resolved signal for the heterocyclic product with that of the internal standard. The reaction time was further prolonged to make sure that full consumption of the substrate was accomplished before starting the next catalytic cycle. After completion of the first cycle, the NMR tube was cooled and a fresh batch of substrate was added without adding any further catalyst and the NMR tube was heated again at 80 °C for 4 h. This process was repeated for four consecutive cycles.

General procedure for the kinetic experiments: All manipulations were performed in a N_2-filled glovebox. Kinetic experiments were performed by using ^{1}H NMR spectroscopy on a JEOL-ECS 400 MHz spectrometer and each rate constant represents an individual kinetic experiment. A standard solution of the catalyst was made by weighing complex **2** into a vial and adding deuterated solvent. Detailed kinetic experiments were performed on the cyclization reactions of compounds **3** and **5**. Stock solutions of compounds **3** and **5**, as well as an internal standard (hexamethylbenzene), were prepared by dissolving them in deuterated solvent in a similar fashion as that described above. The substrates, internal standard, and catalyst were added to a pre-dried screw-capped NMR tube. The NMR tube was sealed, heated at an appropriate temperature, and the progress of the catalysis was monitored by ^{1}H NMR spectroscopy after the described time. The concentrations of the substrate and the product were determined by comparison of the relative integration with a known concentration of hexamethyl benzene that was dissolved in deuterated solvent.

X-ray crystallography of complexes 1 and 2: A suitable crystal of complex **1** was mounted on a glass fiber and the data was collected on an IPDS II Stoe image-plate diffractometer (graphite-monochromated $Mo_{K\alpha}$ radiation, $\lambda = 0.71073$ Å) at 133(2) K. The data were integrated with X-area. The data of complex **2** were collected from a shock-cooled crystal at 100 K on a Bruker SMART-APEX II diffractometer with a D8 goniometer that was equipped with a fine-focus INCOATEC Mo-microsource.[26] The structures were solved by using direct methods (SHELXS-97)[27] and refined by full-matrix least-square methods against F^2 (SHELXL-97).[27] All non-hydrogen atoms were refined with anisotropic displacement parameters. The hydrogen atoms were refined isotropically on calculated positions by using a riding model. No restraints were used. CCDC-870913 (**1**) and CCDC-870914 (**2**) contain the supplementary crystallographic data for this paper. These data can be obtained free of charge from The Cambridge Crystallographic Data Centre via www.ccdc.cam.ac.uk/data_request/cif.

Computational details: Geometry optimizations, transition-state (TS) calculations, and vibrational-frequency analyses were carried out without any symmetry constraints at the level of density functional theory (DFT)-based methods, as implemented in the electronic-structure program Gaussian 03.[28] We used the Beck's three-parameter hybrid-exchange functional[29] combined with the Lee–Yang–Parr nonlocal-correlation function,[30] abbreviated as B3LYP. The split-valence basis set with diffuse functions, namely 6–311++G, was employed for all atoms. We used 6-311++G basis sets for transition-state calculations. Vibrational frequencies were calculated for optimized molecular structures to verify that no negative frequencies were present for the minimum-energy structures and one negative frequency were present for the TS structures.

Acknowledgements

A.M. and T.K.S. are thankful to the IISER-Kolkata and the CSIR, India, respectively, for research fellowships. S.K.M. thanks the CSIR (Sanction Grant No. 01(2369)/10/EMR-II), India, for financial support. P.K.G. thanks the DST, India, for financial support. S.K.M. thanks NMR and X-ray facilities at IISER-Kolkata, and also thanks Prof. H. W. Roesky for his support and constant encouragement.

[1] a) T. E. Müller, K. C. Hultzsch, M. Yus, F. Foubelo, M. Tada, *Chem. Rev.* **2008**, *108*, 3795–3892; b) J. F. Hartwig, *Nature* **2008**, *455*, 314–322; c) K. C. Hultzsch, *Adv. Synth. Catal.* **2005**, *347*, 367–391; d) K. C. Hultzsch, *Org. Biomol. Chem.* **2005**, *3*, 1819–1824; e) P. W. Roesky, T. E. Müller, *Angew. Chem.* **2003**, *115*, 2812–2814; *Angew. Chem. Int. Ed.* **2003**, *42*, 2708–2710; f) T. E. Müller, M. Beller, *Chem. Rev.* **1998**, *98*, 675–703; g) S. Hong, T. J. Marks, *Acc. Chem. Res.* **2004**, *37*, 673–686; h) R. Severin, S. Doye, *Chem. Soc. Rev.* **2007**, *36*, 1407–1420.

[2] a) J. F. Dunne, D. B. Fulton, A. Ellern, A. D. Sadow, *J. Am. Chem. Soc.* **2010**, *132*, 17680–17683; b) M. R. Crimmin, M. Arrowsmith, A. G. M. Barrett, I. J. Casely, M. S. Hill, P. A. Procopiou, *J. Am. Chem. Soc.* **2009**, *131*, 9670–9685; c) A. G. M. Barrett, C. Brinkmann, M. R. Crimmin, M. S. Hill, P. Hunt, P. A. Procopiou, *J. Am. Chem. Soc.* **2009**, *131*, 12906–12907; d) M. R. Crimmin, I. J. Casely, M. S. Hill, *J. Am. Chem. Soc.* **2005**, *127*, 2042–2043; e) S. Datta, P. W. Roesky, *Organometallics* **2007**, *26*, 4392–4394; f) X. Zhang, T. J. Emge, K. C. Hultzsch, *Angew. Chem.* **2012**, *124*, 406–410; *Angew. Chem. Int. Ed.* **2012**, *51*, 394–398; g) C. Brinkmann, A. G. M. Barrett, M. S. Hill, P. A. Procopiou, *J. Am. Chem. Soc.* **2012**, *134*, 2193–2207; h) J. Koller, R. G. Bergman, *Chem. Commun.* **2010**, *46*, 4577–4579.

[3] a) B. D. Stubbert, T. J. Marks, *J. Am. Chem. Soc.* **2007**, *129*, 6149–6167; b) B. D. Stubbert, T. J. Marks, *J. Am. Chem. Soc.* **2007**, *129*, 4253–4271; c) S. Hong, S. Tian, M. V. Metz, T. J. Marks, *J. Am. Chem. Soc.* **2003**, *125*, 14768–14783; d) V. M. Arredondo, S. Tian, F. E. McDonald, T. J. Marks, *J. Am. Chem. Soc.* **1999**, *121*, 3633–3639; e) D. V. Gribkov, K. C. Hultzsch, F. Hampel, *J. Am. Chem. Soc.* **2006**, *128*, 3748–3759.

[4] a) K. Manna, S. Xu, A. D. Sadow, *Angew. Chem.* **2011**, *123*, 1905–1908; *Angew. Chem. Int. Ed.* **2011**, *50*, 1865–1868; b) M. C. Wood, D. C. Leitch, C. S. Yeung, J. A. Kozak, L. L. Schafer, *Angew. Chem.* **2007**, *119*, 358–362; *Angew. Chem. Int. Ed.* **2007**, *46*, 354–358; c) D. C. Leitch, P. R. Payne, C. R. Dunbar, L. L. Schafer, *J. Am. Chem. Soc.* **2009**, *131*, 18246–18247; d) L. E. N. Allan, G. J. Clarkson, D. J. Fox, A. L. Gott, P. Scott, *J. Am. Chem. Soc.* **2010**, *132*, 15308–15320; e) P. D. Knight, I. Munslow, P. N. O'Shaughnessy, P. Scott, *Chem. Commun.* **2004**, 894–895; f) J. A. Bexrud, J. D. Beard, D. C. Leitch, L. L. Schafer, *Org. Lett.* **2005**, *7*, 1959–1962; g) D. C. Leitch, R. H. Platel, L. L. Schafer, *J. Am. Chem. Soc.* **2011**, *133*, 15453–15463; h) L. D. Julian, J. F. Hartwig, *J. Am. Chem. Soc.* **2010**, *132*, 13813–13822; i) Z. Liu, J. F. Hartwig, *J. Am. Chem. Soc.* **2008**, *130*, 1570–1571; j) Z. Liu, H. Yamamichi, S. T. Madrahimov, J. F. Hartwig, *J. Am. Chem. Soc.* **2011**, *133*, 2772–2782; k) K. D. Hesp, S. Tobisch, M. Stradiotto, *J. Am. Chem. Soc.* **2010**, *132*, 413–426; l) B. M. Cochran, F. E. Michael, *J. Am. Chem. Soc.* **2008**, *130*, 2786–2792; m) C. F. Bender, R. A. Widenhoefer, *J. Am. Chem. Soc.* **2005**, *127*, 1070–1071; n) Z. J. Wang, D. Benitez, E. Tkatchouk, W. A. Goddard III, F. D. Toste, *J. Am. Chem. Soc.* **2010**, *132*, 13064–13071; o) U. Nettekoven, J. F. Hartwig, *J. Am. Chem. Soc.* **2002**, *124*, 1166–1167.

[5] R. H. Prince, *Adv. Inorg. Chem. Radiochem.* **1979**, *22*, 349–440.

[6] a) A. Zulys, M. Dochnahl, D. Hollmann, K. Löhnwitz, J.-S. Herrmann, P. W. Roesky, S. Blechert, *Angew. Chem.* **2005**, *117*, 7972–7976; *Angew. Chem. Int. Ed.* **2005**, *44*, 7794–7798; b) M. Dochnahl, K. Löhnwitz, J.-W. Pissarek, M. Biyikal, S. R. Schulz, S. Schön, N. Meyer, P. W. Roesky, S. Blechert, *Chem. Eur. J.* **2007**, *13*, 6654–6666; c) M. Dochnahl, K. Löhnwitz, A. Lühl, J. W. Pissarek, M. Biyikal, P. W. Roesky, S. Blechert, *Organometallics* **2010**, *29*, 2637–2645; d) J. Jenter, A. Lühl, P. W. Roesky, S. Blechert, *J. Organomet. Chem.* **2011**, *696*, 406–418; e) M. Biyikal, M. Porta, P. W. Roesky, S. Blechert, *Adv. Synth. Catal.* **2010**, *352*, 1870–1875; f) A. Pews-Davtyan, M. Beller, *Chem. Commun.* **2011**, *47*, 2152–2154; g) C. Duncan, A. V. Biradar, T. Asefa, *ACS Catal.* **2011**, *1*, 736–750; h) A. Lühl, H. P. Nayek, S. Blechert, P. W. Roesky, *Chem. Commun.* **2011**, *47*, 8280–8282; i) J.-W. Pissarek, D. Schlesiger, P. W. Roesky, S. Blechert, *Adv. Synth. Catal.* **2009**, *351*, 2081–2085; j) K. Löhnwitz, M. J. Molski, A. Lühl, P. W. Roesky, M. Dochnahl, S. Blechert, *Eur. J. Inorg. Chem.* **2009**, 1369–1375; k) M. Biyikal, K. Löhnwitz, N. Meyer, M. Dochnahl, P. W. Roesky, S. Blechert, *Eur. J. Inorg. Chem.* **2010**, 1070–1081; l) M. Dochnahl, L. Löhnwitz, J.-W. Pissarek, P. W. Roesky, S. Blechert, *Dalton Trans.* **2008**, 2844–2848; m) Y. Yin, W. Ma, Z. Chai, G. Zhao, *J. Org. Chem.* **2007**, *72*, 5731–5736; n) N. Meyer, K. Löhnwitz, A. Zulys, P. W. Roesky, M. Dochnahl, S. Blechert, *Organometallics* **2006**, *25*, 3730–3734; o) M. Dochnahl, J.-W. Pissarek, S. Blechert, K. Löhnwitz, P. W. Roesky, *Chem. Commun.* **2006**, 3405–3407; p) K. Alex, A. Tillack, N. Schwarz, M. Beller, *ChemSusChem* **2008**, *1*, 333–338.

[7] A. Mukherjee, S. Nembenna, T. K. Sen, S. P. Sarish, P. K. Ghorai, H. Ott, D. Stalke, S. K. Mandal, H. W. Roesky, *Angew. Chem.* **2011**, *123*, 4054–4058; *Angew. Chem. Int. Ed.* **2011**, *50*, 3968–3972.

[8] a) R. C. Haddon, *Nature* **1975**, *256*, 394–396; b) M. E. Itkis, X. Chi, A. W. Cordes, R. C. Haddon, *Science* **2002**, *296*, 1443–1445; c) S. K. Pal, M. E. Itkis, F. S. Tham, R. W. Reed, R. T. Oakley, R. C. Haddon, *Science* **2005**, *309*, 281–284; d) S. K. Mandal, M. E. Itkis, X. Chi, S. Samanta, D. Lidsky, R. W. Reed, R. T. Oakley, F. S. Tham, R. C. Haddon, *J. Am. Chem. Soc.* **2005**, *127*, 8185–8196; e) S. K. Mandal, S. Samanta, M. E. Itkis, D. W. Jensen, R. W. Reed, R. T. Oakley, F. S. Tham, B. Donnadieu, R. C. Haddon, *J. Am. Chem. Soc.* **2006**, *128*, 1982–1994.

[9] a) Y. Morita, S. Suzuki, K. Sato, T. Takui, *Nat. Chem.* **2011**, *3*, 197–204; b) R. G. Hicks, *Nat. Chem.* **2011**, *3*, 189–191.

[10] a) A. Mukherjee, T. K. Sen, S. K. Mandal, D. Kratzert, D. Stalke, A. Döring, C. Schulzke, *J. Chem. Sci.* **2011**, *123*, 139–144; b) T. K. Sen, A. Mukherjee, A. Modak, P. K. Ghorai, D. Kratzert, M. Granitzka, D. Stalke, S. K. Mandal, *Chem. Eur. J.* **2012**, *18*, 54–58.

[11] P. W. Roesky, *Chem. Soc. Rev.* **2000**, *29*, 335–345.

[12] A. Mukherjee, M. Nethaji, A. R. Chakravarty, *Polyhedron* **2004**, *23*, 3081–3085.

[13] S. Y. Seo, T. J. Marks, *Chem. Eur. J.* **2010**, *16*, 5148–5162.

[14] M. Gómez-Gallego, M. A. Sierra, *Chem. Rev.* **2011**, *111*, 4857–4963.

[15] L. Ackermann, L. T. Kaspar, A. Althammer, *Org. Biomol. Chem.* **2007**, *5*, 1975–1978.

[16] J. Koller, R. G. Bergman, *Organometallics* **2010**, *29*, 3350–3356.

[17] D. A. Walker, T. J. Woodman, D. L. Hughes, M. Bochmann, *Organometallics* **2001**, *20*, 3772–3776.

[18] a) R. G. Parr, Z. Zhou, *Acc. Chem. Res.* **1993**, *26*, 256–258; b) J. K. Burdett, B. A. Coddens, G. V. Kulkarni, *Inorg. Chem.* **1988**, *27*, 3259–3261.

[19] a) S. Santra, P. Ranjan, P. K. Ghorai, S. K. Mandal, *Inorg. Chim. Acta* **2011**, *372*, 47–52; b) S. C. Sau, S. Santra, T. K. Sen, S. K. Mandal, D. Koley, *Chem. Commun.* **2012**, *48*, 555–557.

[20] a) D. Karshtedt, A. T. Bell, T. D. Tilley, *J. Am. Chem. Soc.* **2005**, *127*, 12640–12646; b) T. E. Müller, M. Grosche, E. Herdtweck, A.-K. Pleier, E. Walter, Y.-K. Yan, *Organometallics* **2000**, *19*, 170–180; c) M. Kawatsura, J. F. Hartwig, *J. Am. Chem. Soc.* **2000**, *122*, 9546–9547; d) J. Ambühl, P. S. Pregosin, L. M. Venanzi, G. Consiglio, F. Bachechi, L. Zambonelli, *J. Organomet. Chem.* **1979**, *181*, 255–269.

[21] a) A. L. Casalnuovo, J. C. Calabrese, D. Milstein, *Inorg. Chem.* **1987**, *26*, 971–973; b) R. L. Cowan, W. C. Trogler, *Organometallics* **1987**, *6*, 2451–2453; c) S. Park, M. P. Johnson, D. M. Roundhill, *Organometallics* **1989**, *8*, 1700–1707; d) D. S. Glueck, L. J. Newman Winslow, R. G. Bergman, *Organometallics* **1991**, *10*, 1462–1479.

[22] a) H. M. Senn, P. E. Blöchl, A. Togni, *J. Am. Chem. Soc.* **2000**, *122*, 4098–4107; b) C. A. Tsipis, C. E. Kefaldis, *Organometallics* **2006**, *25*, 1696–1706; c) C. A. Tsipis, C. E. Kefaldis, *J. Organomet. Chem.* **2007**, *692*, 5245–5255; d) B. F. Straub, R. G. Bergman, *Angew. Chem.* **2001**, *113*, 4768–4771; *Angew. Chem. Int. Ed.* **2001**, *40*, 4632–4635; e) C. Müller, R. Koch, S. Doye, *Chem. Eur. J.* **2008**, *14*, 10430–10436; f) S. Tobisch, *Dalton Trans.* **2006**, 4277–4285; g) S. Tobisch, *Chem. Eur. J.* **2007**, *13*, 4884–4894; h) S. Tobisch, *Chem. Eur. J.* **2008**, *14*, 8590–8602; i) A. Motta, G. Lanza, I. L. Fragala, *Organometallics* **2004**, *23*, 4097–4104; j) S. Tobisch, *Chem. Eur. J.* **2006**, *12*, 2520–2531; k) S. Tobisch, *J. Am. Chem. Soc.* **2005**, *127*, 11979–11988.

[23] a) D. R. Armstrong, A. M. Drummond, L. Balloch, D. V. Graham, E. Hevia, A. R. Kennedy, *Organometallics* **2008**, *27*, 5860–5866; b) D. Nobuto, M. Uchiyama, *J. Org. Chem.* **2008**, *73*, 1117–1120.

[24] A. Guerrero, E. Martin, D. L. Hughes, N. Kaltsoyannis, M. Bochmann, *Organometallics* **2006**, *25*, 3311–3313.

[25] a) P. Horrillo Martínez, K. C. Hultzsch, F. Hampel, *Chem. Commun.* **2006**, 2221–2223; b) G. A. Molander, E. D. Dowdy, *J. Org. Chem.* **1998**, *63*, 8983–8988; c) K. D. Hesp, M. Stradiotto, *Org. Lett.* **2009**, *11*, 1449–1452; d) C. F. Bender, W. B. Hudson, R. A. Widenhoefer, *Organometallics* **2008**, *27*, 2356–2358.

[26] T. Schulz, K. Meindl, D. Leusser, D. Stern, J. Graf, C. Michaelsen, M. Ruf, G. M. Sheldrick, D. Stalke, *J. Appl. Crystallogr.* **2009**, *42*, 885–891.

[27] G. M. Sheldrick, *Acta Crystallogr. Sect. A* **2008**, *64*, 112–122.

[28] M. J. Frish, G. W. Trucks, H. B. Chlegel, et al. GAUSSION 03, Gaussion, Inc., Wallingford, CT, **2004**.

[29] A. D. Becke, *J. Chem. Phys.* **1993**, *98*, 5648–5652.

[30] C. Lee, W. Yang, R. G. Parr, *Phys. Rev. B* **1988**, *37*, 785–789.

Received: March 15, 2012
Published online: ■■ ■■, 0000

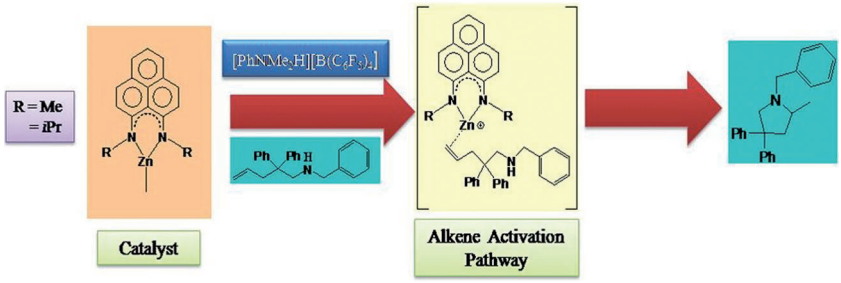

Phenalenyl-based organozinc complexes were used as catalysts for the intramolecular hydroamination reactions of unactivated primary and secondary aminoalkenes. DFT calculations predicted that the organozinc complex followed an alkene-activation pathway for the cyclization of secondary aminoalkenes.

Hydroamination

*A. Mukherjee, T. K. Sen, P. K. Ghorai, P. P. Samuel, C. Schulzke, S. K. Mandal** ..... ■■■■–■■■■

Phenalenyl-Based Organozinc Catalysts for Intramolecular Hydroamination Reactions: A Combined Catalytic, Kinetic, and Mechanistic Investigation of the Catalytic Cycle

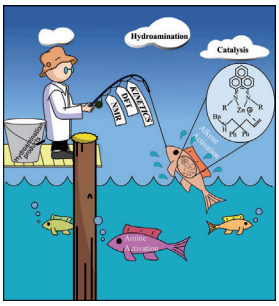

Organozinc Complexes

New phenalenyl-based organozinc complexes were synthesized, characterized, and applied in intramolecular hydroamination reactions of unactivated primary and secondary aminoalkenes. The frontispiece illustrates that the zinc-catalyzed hydroamination of secondary aminoalkene substrates proceeds through the alkene activation pathway ascertained by NMR spectroscopy, kinetic studies, and DFT calculations, which are described in the Full Paper by S. K. Mandal et al. on page ■■ ff.